Zooplankton size and distribution within mesoscale structures in the Mozambique Channel: A comparative approach…

6 authors, including:

Anne Lebourges-Dhaussy
Institute of Research for Development
39 PUBLICATIONS   **331** CITATIONS

SEE PROFILE

Jenny A. Huggett
South Africa Government
45 PUBLICATIONS   **1,124** CITATIONS

SEE PROFILE

Erwan Josse
Institute of Research for Development
103 PUBLICATIONS   **1,208** CITATIONS

SEE PROFILE

Hans M. Verheye
Department of Environmental Affairs
97 PUBLICATIONS   **2,822** CITATIONS

SEE PROFILE

Some of the authors of this publication are also working on these related projects:

Project   ACEP II View project

Project   BIOPELAGOS. Top marine predator organisation in the South Pacific View project

Contents lists available at ScienceDirect

Deep-Sea Research II

CrossMark

Zooplankton size and distribution within mesoscale structures in the Mozambique Channel: A comparative approach using the TAPS acoustic profiler, a multiple net sampler and ZooScan image analysis

A. Lebourges-Dhaussy [a,*], J. Huggett [b,c], S. Ockhuis [d], G. Roudaut [a], E. Josse [a], H. Verheye [b,c]

[a] Institut de Recherche pour le Développement (IRD), UMR LEMAR 195 (UBO/CNRS/IRD/Ifremer), Campus Ifremer, BP 70, 29280 Plouzané, France
[b] Oceans and Coastal Research, Department of Environmental Affairs, Private Bag X2, Roggebaai 8012, Cape Town, South Africa
[c] Marine Research Institute, University of Cape Town, Private Bag X3, Rondebosch 7701, South Africa
[d] Cape Peninsula University of Technology, PO Box 652, Cape Town 8000, South Africa

ARTICLE INFO

ABSTRACT

Two surveys were conducted in the Mozambique Channel in November 2009 and April/May 2010 to study the influence of mesoscale eddies on the zooplanktonic component of the ecosystem. Three complementary methods were used to sample zooplankton: (1) hydro-acoustics with a TAPS™ multi-frequency zooplankton profiler; (2) in situ biological sampling using a Multinet with samples processed via the classical settled biovolume technique; (3) ZooScan image analysis which determines biovolume, size and taxonomic composition. This approach presented an ideal opportunity to compare the results of these different methods which highlighted a large overlap in their detectable size range. Each method favoured a particular size fraction of the population, i.e. TAPS for the microzooplankton (< 0.1 mm ESR) and the Multinet and ZooScan for larger sizes (> 3 mm ESR). In the case of the 2009 cruise, a well-established cyclone–anticyclone dipole was sampled, with results clearly indicating a higher concentration of zooplankton in the cyclonic eddy compared to the anticyclonic counterpart. The TAPS also detected high surface (0–22 m) concentrations of what appeared to be microzooplankton or marine snow in the cyclone. In 2010, the eddy field was less defined and more spatially variable compared to that in 2009. Two cyclonic and anticyclonic features were sampled during the cruise, each with different life histories and levels of stability. Results were inconsistent compared to those of 2009 and dependent on the size component of the population, with both cyclonic and anticyclonic features capable of having higher planktonic biomass. Differences in species composition between these mesoscale features were not too different and mainly a matter of relative biovolume. Less well formed eddy fields, particularly in the mid-Mozambique Channel, therefore appear to result in indistinct vertical and horizontal zooplankton distribution patterns.

1. Introduction

The Mozambique Channel does not have a steady western boundary current (Quartly and Srokosz, 2004) but rather is dominated by southward migrating trains of eddies, particularly large anticyclones with diameters of ∼300 km. The anticyclones are generated at a frequency of approximately four per year, extend to the bottom of the channel (2000–3000 m deep), and propagate southwards at speeds of 3–6 km per day along the western edge of the channel (de Ruijter et al., 2002; Schouten et al., 2003; Backeberg and Reason, 2010). At the southern end of the channel they enter the upstream Agulhas region where they may generate disturbances in the Agulhas Current that result in shedding of Agulhas rings (Schouten et al., 2003; Backeberg and Reason, 2010).

Mesoscale physical features such as fronts or eddies are typically the flow type with the largest kinetic energy in the ocean (besides the tides) (Capet et al., 2008). This mechanical energy may become accessible for augmenting trophic energy available to biological organisms (Bakun, 2006) creating attractive pelagic habitats for higher trophic level marine organisms (Godø et al., 2012). The core upwelling which results from the divergence of the surface water in the cyclonic eddy may vertically transport nutrients into the euphotic zone and facilitate enrichment (McGillicuddy et al., 1998; Oschlies and Garçon, 1998). Anticyclonic eddies, on the other hand, cause local downwelling in the center of the eddy (Bakun, 2006) and may concentrate surface material (Yebra et al., 2005). Various studies have shown the importance of eddies in oligotrophic regions for increasing nutrients and primary productivity (Falkowski et al., 1991; McGillicuddy et al., 1998;

* Corresponding author.
E-mail address: anne.lebourges.dhaussy@ird.fr (A. Lebourges-Dhaussy).

Oschlies and Garçon, 1998; Seki et al., 2001; Tew-Kai and Marsac, 2009; Kolasinski et al., 2012). The periphery of eddies may also be enriched in two ways: the offshore advection and inclusion of shelf waters when cyclonic or anticyclonic eddies pass close to the coast (Machu, 2000; Quartly and Srokosz, 2004); or the accumulation of upwelled deep material from the center of the cyclonic eddy.

Studies in the Mozambique Channel have also shown that frontal areas between eddies can attract top-predators like frigate birds, particularly around cyclones (Weimerskirch et al., 2004; Tew-Kai and Marsac, 2010) that have drawn coastal nutrient-rich waters offshore into the eddy periphery (Sabarros et al., 2009). Consequently, high concentrations of micronekton were found at the eddy periphery with a high probability of encountering large aggregations during the day (Sabarros et al., 2009). An indication of high abundance of micronekton related to a cyclonic feature has also been observed in Hawaiian waters (Drazen et al., 2001). In the central Gulf of Mexico, a comparison of a biomass proxy from processed ADCP data collected in a cold-core mesoscale feature separating two warm-core features, showed that the cold-core region was a zone of local aggregation of zooplankton and micronekton (Zimmerman and Biggs, 1999). The opposite observation has also been made in the Indian Ocean off Western Australia, however, where microzooplankton biomass was clearly higher in a warm-core eddy than in a cold-core counter-part (Paterson et al., 2007). Studies on zooplankton and micronekton in these areas are limited and the exact mechanisms of the eddy-induced effects are still controversial (Gruber et al., 2011). There are also few reports on the vertical stratification of organisms in eddies and Muhling et al. (2007), for example, demonstrated a stronger vertical structure of ichthyoplankton assemblages in a cold-core eddy than in a warm-core eddy.

There is a real need to assess zooplankton patterns at finer scales in relation to hydrographic conditions. The objective of this paper therefore was to investigate the vertical and horizontal distribution of zooplankton across the mesoscale eddy fields in the Mozambique Channel, including community structure in terms of both size and assemblage. The key question posed is whether cyclonic or anticyclonic eddies have the greatest impact on zooplankton distribution, or are there rather other phenomena on a smaller scale? The sampling approach included a Multinet zooplankton sampler coupled with an acoustic zooplankton profiler (TAPS™), a technique used for the first time in the Mozambique Channel. Since there are differences between the two techniques, a comparison of methods is also discussed in order to clarify variations in the results from acoustics and those from the Multinet.

2. Methods

2.1. Equipment and survey protocol

The data considered here originate from two cruises on the RV *Antea* in the Mozambique Channel. The first cruise MC09B during November 2009 was concentrated in the southwestern sector of the channel (23.4°S–25.1°S; 35.8°E–38°E) to study a cyclone–anticyclone pair (Fig. 1A). The second cruise MC10A during April/May 2010 was spatially more extensive and located mostly in the center of the channel (15°S–22°S; 39.2°E–43°E) (Fig. 1A). This cruise had two parts with different scientific objectives. Leg 1 was dedicated to the study of trophic relationships, i.e. phytoplankton to top predators such as tuna. Leg 2 was designed to investigate primary and secondary production processes. The strategy was to sample along a transect at high spatial resolution (27 km between stations) through a well-established dipole.

During these cruises, acoustic data were acquired from two types of equipment. The continuous data collected by the SIMRAD ER60 echosounder is reported by Béhagle et al. (2014). This paper focuses on the multi-frequency data collected by the TAPS-6™ (Tracor Acoustic Profiling System) profiler over a maximum depth of 200 m. The TAPS-6™ operates at six high frequencies (265, 420, 710, 1100, 1850, 3000 kHz) and is designed to detect micro- and mesozooplankton (Holliday and Pieper, 1980). Unfortunately, the lowest frequency malfunctioned during both cruises as did the 1850 kHz frequency at several of the stations in 2010. A total of 14 and 35 profiles were acquired during the MC09B and MC10A cruises respectively, in different types of mesoscale structures.

Acoustic data were acquired together with temperature, salinity and oxygen measurements using a CTD profiler (SBE 911) and light data from a PAR (Photosynthetically Active Radiation) sensor. Water samples were drawn for analysis of discrete chlorophyll *a* concentrations as the fluorescence profile data for MC09B and MC10A were found to be unreliable (Lamont et al., 2014). Zooplankton sampling was conducted using a Hydrobios Multinet type Midi (200 μm mesh, 0.25 m^2 mouth area). The Multinet was towed obliquely at a speed of $\sim$1 m s^{-1} from a depth of 200 m to the surface, collecting zooplankton samples from five depth layers. The TAPS-6™ instrument was mounted on the Multinet. All zooplankton samples were fixed and preserved with 4% formaldehyde (v/v), buffered with CaCO$_3$, and stored in plastic jars for later taxonomic and dry weight analysis as reported by Huggett (2014).

2.2. Data processing

The size range explored in the inversion process of the TAPS-6 acoustic data was 0.05–3 mm. The basic algorithm used to process the multi-frequency data was an inversion algorithm (Holliday, 1977a; Greenlaw and Johnson, 1983; Holliday and Pieper, 1995), with the non-negative least-squares (NNLS) method most commonly used (Lawson and Hanson, 1974). A review of the literature shows that this approach has been successfully applied to small zooplankton (Holliday et al., 1989; Pieper et al., 1990; Costello et al., 1989; Napp et al., 1993; Lebourges-Dhaussy et al., 2009), krill (Greenlaw, 1979), mesopelagic fishes (Kalish et al., 1986), and epipelagic fishes (Holliday, 1977b, 1985).

The TAPS-6 was deployed in "cast mode", with the TAPS-6 in a horizontal position, profiling the water column at a descent speed of 0.5 m s^{-1} and sampling a small volume of $\sim$5 L at each ping. This enabled a focus on small and abundant organisms such as copepods, with the larger and less abundant plankton such as euphausiids having less chance to pass through this small volume (Pieper et al., 2001). Data acquisition was centered at 1.3 m from the TAPS-6 transmitting surface, with each ping resulting in an average of five sampling points at and around this central position. The ping rate was 2.63 pings s^{-1} and the acquisition configuration was set to an average of four pings per data sample at a given depth in 2009, but at one ping in 2010. Vertical binning of the data was used to obtain regularly spaced values for a final vertical resolution of 1 m. This resulted in a new average of $\sim$2 samples per binned data during 2009, and a new average of $\sim$8 samples per binned data in 2010. Each Sv (volume backscattering strength) data point finally obtained was therefore the average of $\sim$40 samples. The inversion algorithm (Greenlaw, 1979) requires input from a model for the acoustic backscattering of small zooplankton organisms such as copepods. For the cast mode used here, where the sampled volume is small ($\sim$5 L), the truncated fluid sphere (TFS) model (Holliday, 1992) is most appropriate. The settings for *g* (density contrast between the organism and its surrounding water) and *h* (sound velocity contrast between the organism and its surrounding water) (Greenlaw and Johnson, 1982) were set to
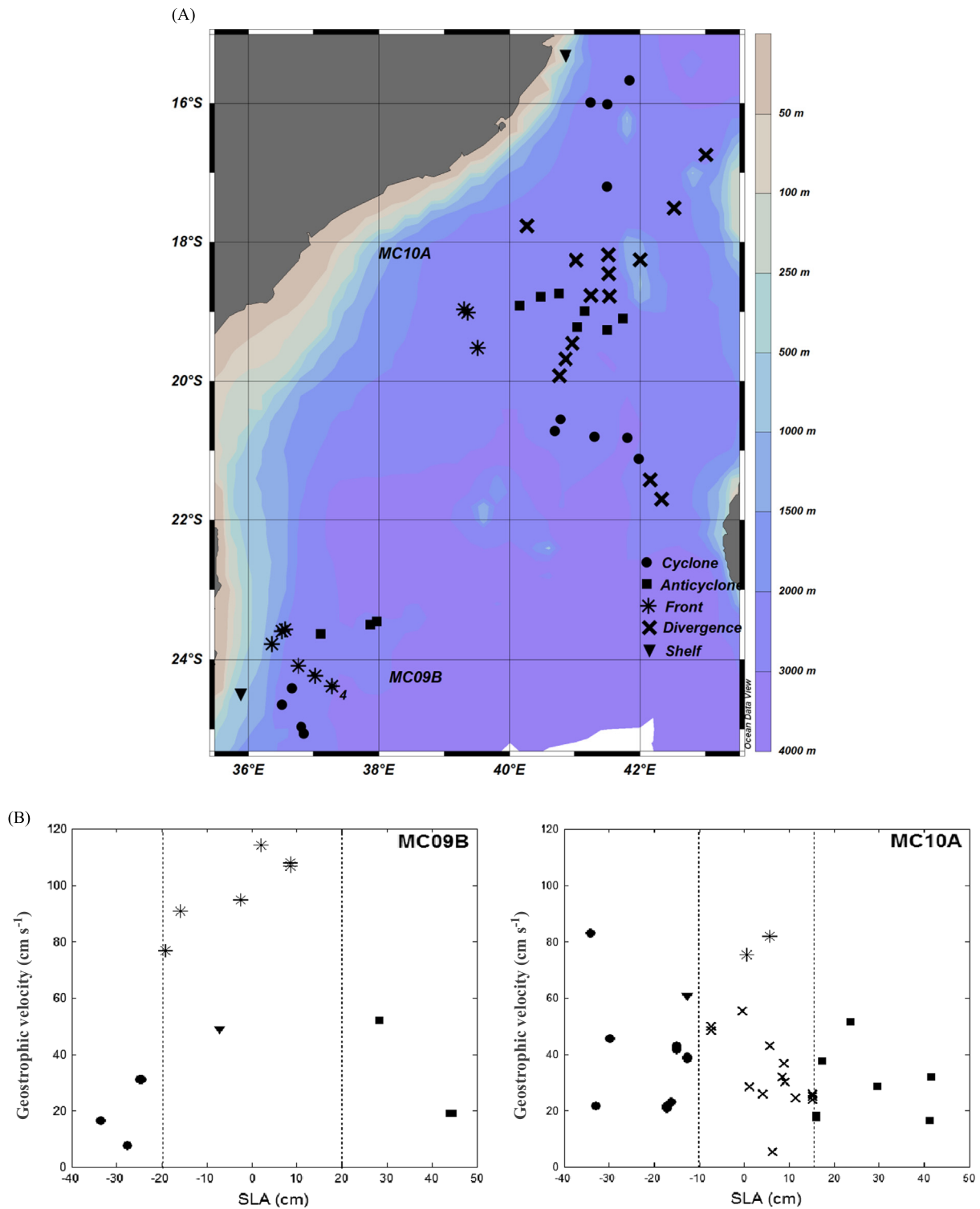
Fig. 1. (A) Location of the TAPS stations during both cruises with corresponding mesoscale classification. Frontal station 4 of the MC09B survey is indicated in the southwest. Color contours indicate bathymetry. (B) Geostrophic velocity versus SLA for TAPS stations in 2009 and (C) in 2010, including mesoscale classification.

the values determined by Holliday (1992) ($g=1.12$, $h=1.09$). Comparisons of biovolumes with the biological Multinet sampling were in accordance with these parameter settings in a previous study on the South African shelf similarly performed with five frequencies from 420 kHz to 3 MHz (Lebourges-Dhaussy et al., 2009). The vertical resolution of the zooplankton profiles was 1 m, similar to the physical parameters, enabling small scale vertical observations to be made. The data analysis provided profiles of biovolume per class of equivalent spherical radius (ESR) and the

number of classes retained must be no higher than the number of available frequencies. As a result of the malfunction of the 265 kHz frequency and sometimes of the 1850 kHz frequency, as well as the global size distribution obtained, the following four classes of ESR were defined for both cruises: 0–0.2 mm, 0.2–0.5 mm, 0.5–1 mm, and 1–3 mm.

A discriminant function analysis performed on sea level anomalies (SLA), geostrophic velocities and high-resolution bathymetry was used to classify each station as cyclonic (C), anticyclonic (A),

divergence (D), frontal (F) or shelf (S), as described by Lamont et al. (2014). The number of TAPS stations per mesoscale structure and time of day for each cruise is shown in Table 1. The spatial distribution of stations is shown in Fig. 1A, highlighting the area sampled by MC09B being much further south than MC10A. Note that there were no divergence stations sampled in 2009, few frontal stations in 2010, and both cruises had only one shelf station. The relationship between geostrophic velocity and SLA for each station during both surveys is shown in Fig. 1B.

2.3. Image analysis of zooplankton

Zooplankton samples, or aliquots, from the Multinet were subjected to image analysis using the Hydroptic ZooScan. The overall approach, which includes sample preparation, scanning with ZooScan hardware and image processing with ZooProcess and Plankton Identifier software, followed procedures described by Gorsky et al. (2010). These authors also discuss the building and validation of training sets, the selection of classification algorithms and the accuracy of body size and biomass estimations that can be derived from the ZooScan system.

Each scanned raw 16-bit gray image recorded by ZooProcess was normalized and converted to an 8-bit source image from which the background blank image was subtracted. After automatic removal of objects touching the sides of the frame, this final image was used for object detection and the extraction of measurement variables from each detected object. By default, only objects having an ESR of > 0.15 mm were detected and processed. All images were checked for background subtraction and correct object contours by viewing segmented black and white images.

A learning set of selected categories was then created, which each contained digital images of individual objects of similar visual appearance (i.e. vignettes). Each folder represented a taxonomic group of organisms (e.g. copepods, chaetognaths, ostracods, etc.) or abiotic objects (e.g. bubbles, fibers and detritus) that were visually 'dragged-and-dropped' into the relevant folder. Exactly 200 such vignettes were extracted from each scanned image. This learning set was then used for the automatic classification of objects by applying the Random Forest classifier within Plankton Identifier, interfaced with ZooProcess, across all scanned images. The vignettes were subsequently validated (using XnView) by checking the automatic sorting and making corrections when necessary (i.e. by manually dragging incorrectly classified objects to the correct folder). Measurements of major and minor axes (mm) of each object were used to calculate biovolume (mm^3) based on ESD, where ESD volume $= 4/3\pi(\text{Area}/\pi)3/2$.

Table 1
Distribution of the stations for each mesoscale feature and time of day.

Survey/structure	Cyclone	Anticyclone	Front	Divergence	Shelf	N
MC09B	4	3	6	–	1	14
Day	1	2	4	–	–	7
Night	3	1	2	–	1	7
MC10A	10	7	2	14	1[a]	34
Day	6	4	2	9	–	21
Night	4	3		5	–	12

[a] Transition period.

3. Results

3.1. Hydrographic structure of mesoscale features

3.1.1. MC09B survey

Each mesoscale feature in 2009 corresponded to typical profiles as shown for temperature in Fig. 2. The depth of the mixed layer (MLD) differed considerably between features, as did the slope of the thermocline, but surface temperatures were similar for all structures (25–26 °C). Apart from the deeper mixed layer in anticyclonic features, anticyclonic and frontal profiles were quite
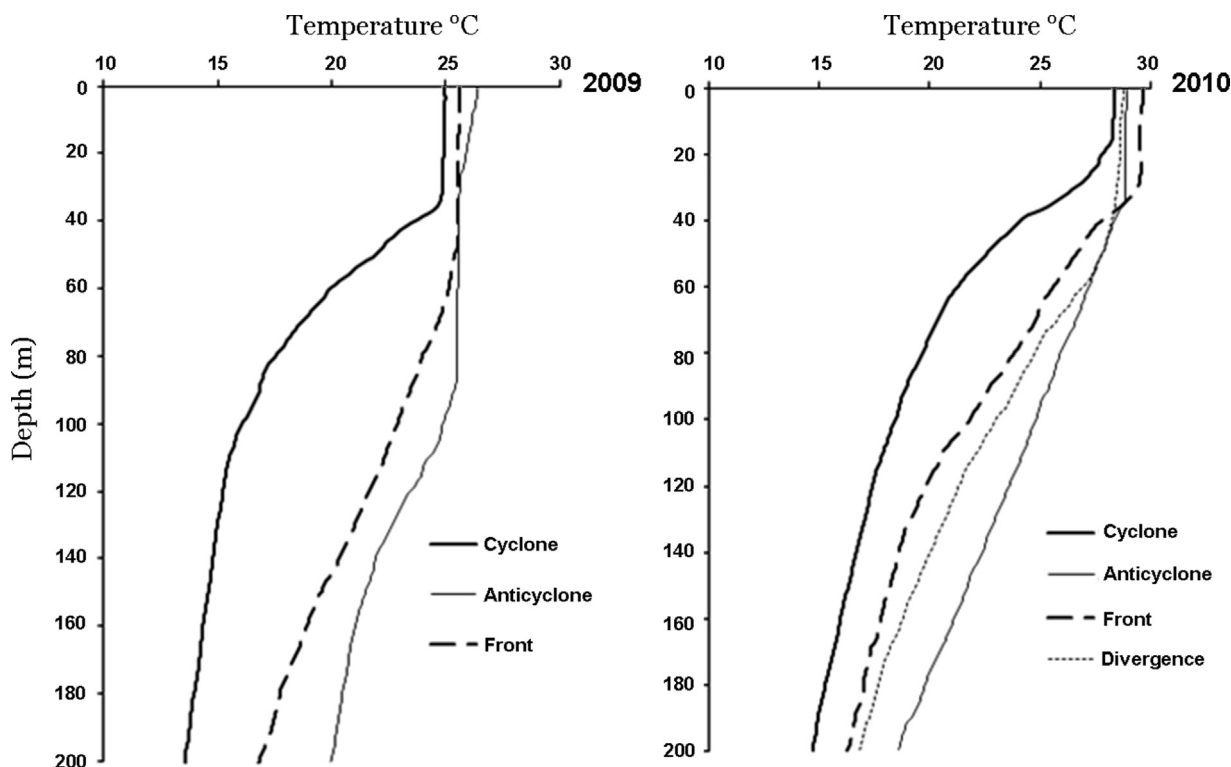

Fig. 2. Mean temperature profiles for each mesoscale feature in 2009 and 2010.

similar. Cyclonic profiles differed strongly from the others with a much shallower mixed layer (Fig. 2). There was a highly significant positive correlation between the SLA and the MLD ($r^2 = 0.91$, $p \ll 0.001$, Fig. 3). The depth of maximum chlorophyll concentration increased from cyclonic (40–50 m) to frontal (60–120 m) to anticyclonic features (105–120 m) (Table 2). The chlorophyll maxima were similar for cyclonic and anticyclonic stations and higher than for frontal stations (Table 2). Both surface and integrated chlorophyll concentrations were clearly higher at anticyclonic stations compared with cyclonic and frontal stations (Table 2). Station 4 (24.5°S, 37.5°E, Fig. 1A) stands out from other frontal stations in that it had a shallow mixed layer (46 m compared to 60–75 m) and a fairly shallow and strong chlorophyll maximum (60 m, 0.73 mg m^{-3}).

3.1.2. MC10A survey

Station classification procedure was the same as for 2009, but for 2010 the variability within each group of profiles was higher, leading to less contrast in the hydrography between features (Fig. 2). Surface temperature varied between the mesoscale structures, but remained between 27 °C and 30 °C for all of them, i.e. much warmer than during the MC09B cruise (Fig. 2). Although the MLD was shallower for the cyclonic structures, the difference in MLD between structures was less marked in 2010 than in 2009 (Figs. 2 and 3) and all four structures in 2010 had some stations with a relatively shallow mixed layer (Fig. 3). There was also a positive correlation between the SLA and the MLD but it was weaker and less significant ($r^2 = 0.16$, $p = 0.014$, Fig. 3). In each structure two groups of stations were apparent, those with surface

temperatures of ~30 °C for one group and 28 °C for the other group, corresponding to Leg 1 and Leg 2 of the cruise respectively. As in 2009, the depth of the chlorophyll maximum in 2010 varied from shallow at cyclonic stations (25–60 m), to intermediate at frontal (60–80 m) and divergence stations (40–95 m), to deep at anticyclonic stations (75–120 m) (Table 2). On average, maximum chlorophyll concentrations were highest in the cyclonic and frontal structures, but lower at divergence and anticyclonic stations (Table 2). Peak integrated chlorophyll concentrations were observed at the cyclonic stations, with lower but similar values found in the three other structures (Table 2). There was a gradual decrease in the average surface chlorophyll concentration from cyclonic to divergence to anticyclonic to frontal stations (Table 2).

3.2. Integrated biovolume and size composition

To assess the effect of losing the 1850 kHz for some of the stations, the results obtained with inversions based on 5 and on 4 frequencies were compared. The biovolume profiles obtained were identical and the mean biovolume, as well as the patterns provided by each inversion configuration by size class, were very close (Fig. 4). Considering the possible presence of surface bubbles and thus the lack of surface values for some stations, the common depth range for which data is available is 22–200 m. Comparisons on integrated values are thus valid for this depth range. However, for stations where the mixed layer was shallow, the surface layer may be important and therefore two calculations are presented, although there were a variable number of samples in the upper 0–22 m.
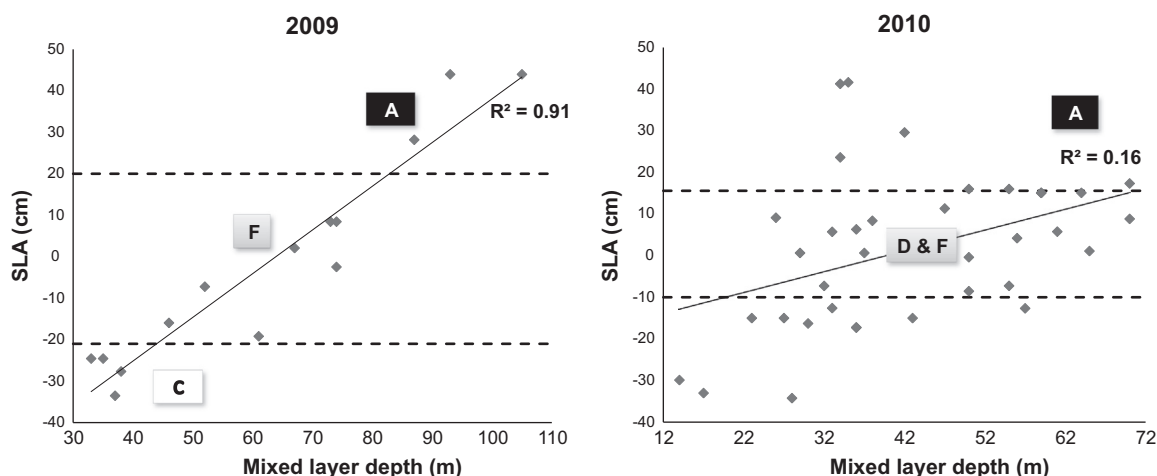

Fig. 3. Relationships between the depth of the mixed layer and SLA for 2009 and 2010. Dashed lines indicate the SLA thresholds separating the features, inferred from the DFA classification and from station distributions in Fig. 1B and C.

Table 2
Mean values ($\pm$ confidence interval) of chlorophyll characteristics for each mesoscale feature. A=anticyclone, C=cyclone, F=frontal, D=divergence.

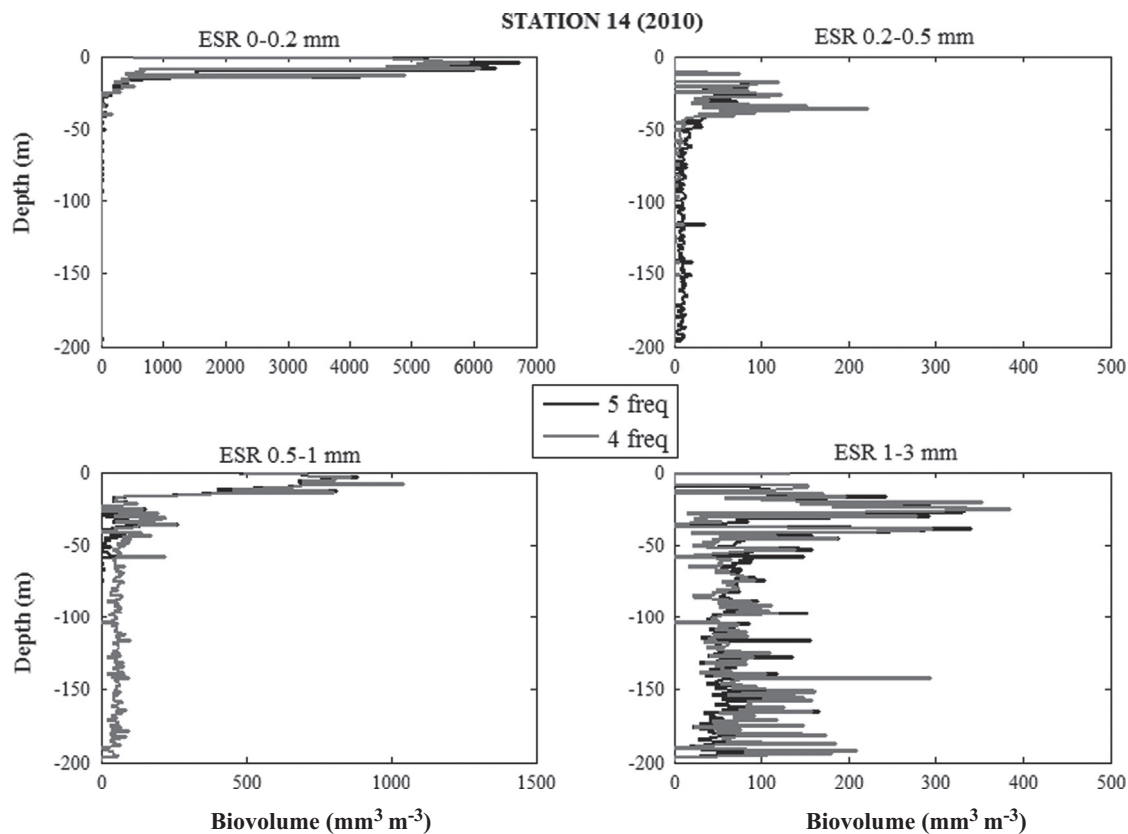|	A	C	F	D
MC09B				
Chl maximum (mg m^{-3})	0.67 (± 0.03)	0.62 (± 0.09)	0.51 (± 0.18)	
Surface Chl (mg m^{-3})	0.28 (± 0.005)	0.15 (± 0.03)	0.1 (± 0.05)	
Integrated Chl (mg m^{-2})	67.9 (± 5.1)	26.7 (± 0.8)	34.4 (± 8.4)	
Depth range of Chl maximum (m)	105–120	40–50	60–120	
MC10A				
Chl maximum (mg m^{-3})	0.38 (± 0.04)	0.61 (± 0.07)	0.6 (± 0.07)	0.46 (± 0.04)
Surface Chl (mg m^{-3})	0.23 (± 0.06)	0.25 (± 0.07)	0.2 (± 0.01)	0.24 (± 0.07)
Integrated Chl (mg m^{-2})	41.9 (± 2.3)	52.4 (± 14.8)	42.9 (± 6.0)	42.6 (± 3.7)
Depth range of Chl maximum (m)	75–120	25–60	60–80	40–95

Fig. 4. Comparison of data obtained with the inversion algorithm for four (420, 700, 1100, 3000 kHz) and five (420, 700, 1100, 1850, 3000 kHz) frequencies at station 14 for cruise MC10A.

3.2.1. Comparison of methods

Biovolumes obtained by the three methods (total settled volume (TSV), ZooScan derived biovolume and TAPS derived biovolume) on a station basis are shown in Fig. 5. In 2009, TSV-derived biovolumes were generally much higher compared to those from the other methods (Fig. 5A). This is because the TSV method overestimated true biovolume as a result of interstitial spaces between settled organisms in the measuring cylinder. Additional bias may have been introduced by the presence of different shaped organisms (Hagen, 2000). Disparity between methods was also observed when a large concentration of very small particles was detected by the TAPS, resulting in a high TAPS biovolume compared to that estimated by the ZooScan (eg C1, C13, Fig. 5A). In these cases the mean TAPS biovolume using only particles with an ESR > 0.2 mm was closest to that obtained by the ZooScan. In the case of the two frontal stations where the largest size class dominated the ZooScan biovolume (F9, F11, Fig. 5A), the large difference between the ZooScan and the TAPS (> 0.2 mm data) was reduced by removing the > 3 mm class from the ZooScan calculation. However, for the remaining stations, removing the > 3 mm class resulted in an underestimation relative to TAPS derived biovolume (Fig. 5A).

Overall in 2009, there was a highly significant correlation between the ZooScan and TSV biovolumes ($R = 0.75$, $p = 0.001$). Comparing the TAPS and TSV results, a better correlation was obtained with the TAPS > 0.2 mm data ($R = 0.50$, $p = 0.08$) than with the TAPS total data ($R = 0.42$, $p = 0.15$). This was also reflected in the ZooScan results where TAPS total yielded $R = 0.44$ ($p = 0.18$) and TAPS > 0.2 mm was $R = 0.59$ ($p = 0.06$). The correlation was even stronger when the ESR > 3 mm size class was removed from the ZooScan calculations, resulting in $R = 0.69$ ($p = 0.02$) for ZooScan < 3 mm with TAPS > 0.2 mm. The correlation between TAPS > 0.2 mm and the ZooScan was much stronger if the total

ZooScan values were utilized for all stations except the frontal F9 and F11 stations, where the ZooScan < 3 mm biovolume was used (indicated with arrows on Fig. 5A); without these two sets of values, the correlation increased to $R = 0.91$ ($p \ll 0.001$).

Similarly in 2010, the TSV-derived biovolumes were greater than most values obtained by the other methods, although there were some exceptions where the TAPS data was higher than those from TSV (eg C14, D10, Fig. 5B), or the ZooScan showed the highest biovolumes (C36, D9; Fig. 5B). For all these exceptions, the smallest size class was the main contributor to the high TAPS values, with the largest size class contributing substantially to the high ZooScan values. It is difficult to detect common trends between the methods from the data in Fig. 5B. The only significant correlation was between the ZooScan total and the TSV data ($R = 0.56$, $p = 0.004$). This correlation is weaker than that obtained for the 2009 data as the TSV curve deviated from that of the ZooScan at stations C36 and D9. Without those two points, the correlation increased to 0.81. There were closer similarities between the data series that included TAPS > 0.2 mm, ZooScan total and ZooScan < 3 mm biovolumes (Fig. 5C). TAPS > 0.2 mm data were usually closer to the ZooScan total than the ZooScan < 3 mm data, except for some stations with a high contribution from the larger organisms. The high ZooScan biovolumes at stations C36 and D9 prevented any significant correlation between the TAPS and ZooScan data. Without these two points, the correlations between the TAPS > 0.2 mm and both the ZooScan total and the ZooScan < 3 mm were marginally significant ($p < 0.1$), with coefficients of 0.36 and 0.38 respectively. However, a much higher correlation ($R = 0.69$, $p = 0.0003$) was achieved between the TAPS > 0.2 mm data and a curve using the ZooScan total data, except for certain stations (marked with vertical arrows on Fig. 5C) where the ZooScan < 3 mm values were used instead. No correlation was found between the TAPS > 0.2 mm and the TSV data for 2010.
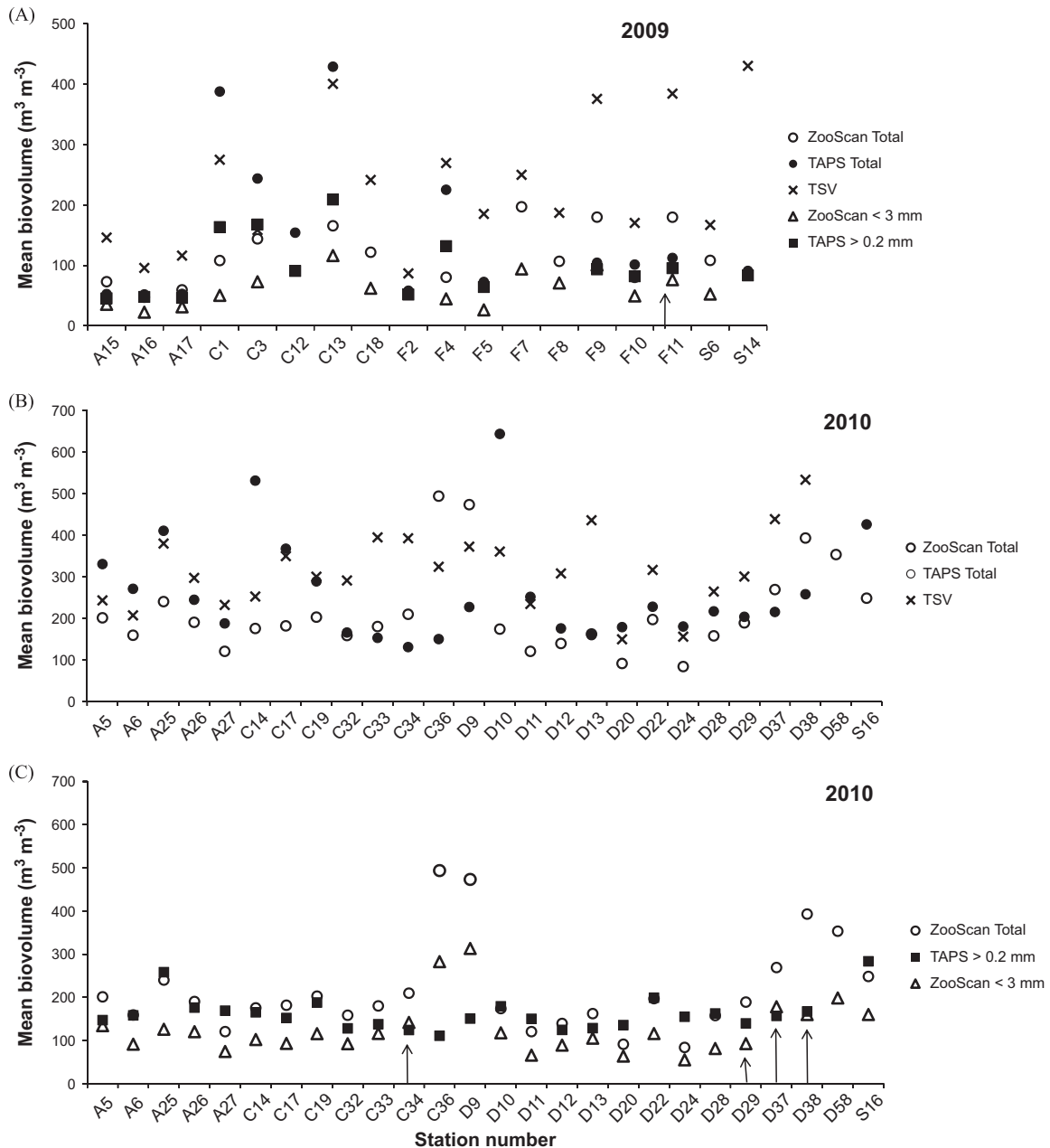
Fig. 5. Comparison of the mean water column biovolumes obtained for each station, using the ZooScan, TAPS and settled volume (TSV) for (A) 2009 and (B, C) 2010. Also included are TAPS data with ESR > 0.2 mm and ZooScan data with ESR < 3 mm.

3.2.2. Mesoscale effects

Patterns of micro- and mesozooplankton organization at small spatial and temporal scales are stochastic, unpredictable and immeasurable, and it is therefore necessary to utilize averaging and rate calculations to obtain representative patterns (Zhou, 2006). Yearly data appears to have an impact on integrated biovolume, irrespective of the method used (Fig. 6), as biovolumes were higher in 2010 than in 2009 (ANOVA $p < 0.01$ for all methods) as confirmed by Huggett (2014).

Different biovolume patterns in relation to mesoscale structures were observed for the two years (Fig. 7). In 2009, anticyclonic stations were the lowest for all methods, frontal stations had medium biovolume, and cyclonic stations displayed the highest mean biovolume (Fig. 7A). Interestingly, according to a multiple comparison test based on an analysis of variance, including a Bonferroni adjustment to compensate for multiple comparisons, the only significant difference ($p < 0.05$) was found between the

cyclonic and the anticyclonic features using the TAPS 22–200 m data. There was also very high biovolume at the surface (0–22 m) in the cyclonic structures, related to shallow mixed layers, but low surface biovolume in the other features.

In contrast to 2009, the TAPS results for 2010 indicated lowest mean biovolume at cyclonic and divergence stations, with higher biovolume in anticyclonic and frontal structures (Fig. 7B). Frontal structure was represented by only two stations and therefore any differences with the other features were not significant. These two stations exhibited high surface concentrations of zooplankton in their shallow mixed layer, with surface concentrations also high at the anticyclonic and cyclonic stations. Greatest variability occurred in the latter. The pattern inferred from the TAPS data contrasted with that from the nets (TSV and ZooScan), for which mean biovolume within the anticyclonic feature was less than or equal to the mean biovolumes in cyclonic and divergence features. For the nets however, following the same multiple comparison tests as
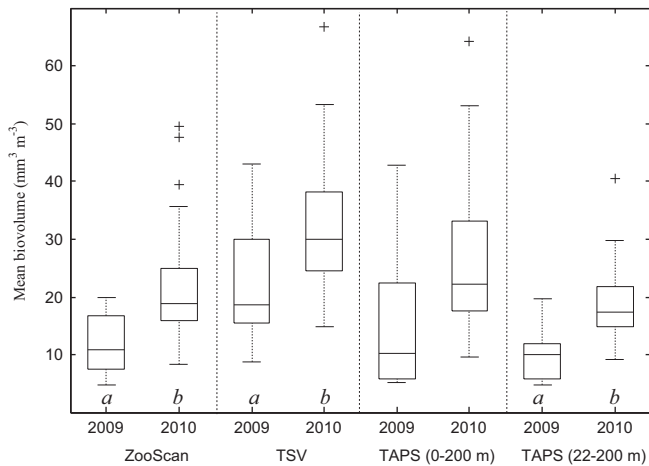
Fig. 6. Boxplots of mean biovolumes for the three methods during 2009 and 2010, where *a* and *b* indicate significantly different means.
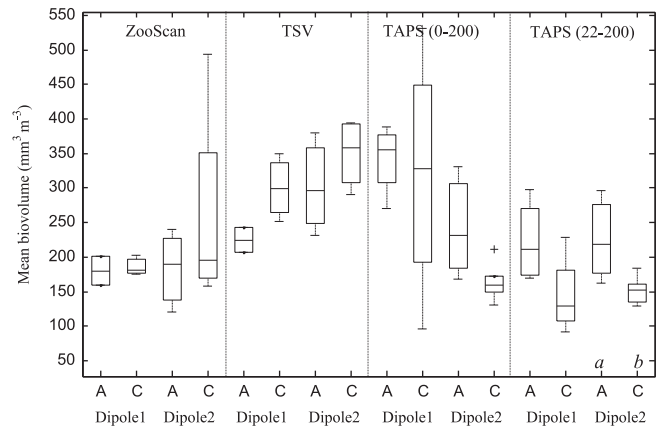

Fig. 8. Boxplots of mean biovolumes for the three methods for cyclones (C) and anticyclones (A) in 2010, comparing dipole 1 and dipole 2, where *a* and *b* indicate significantly different means.
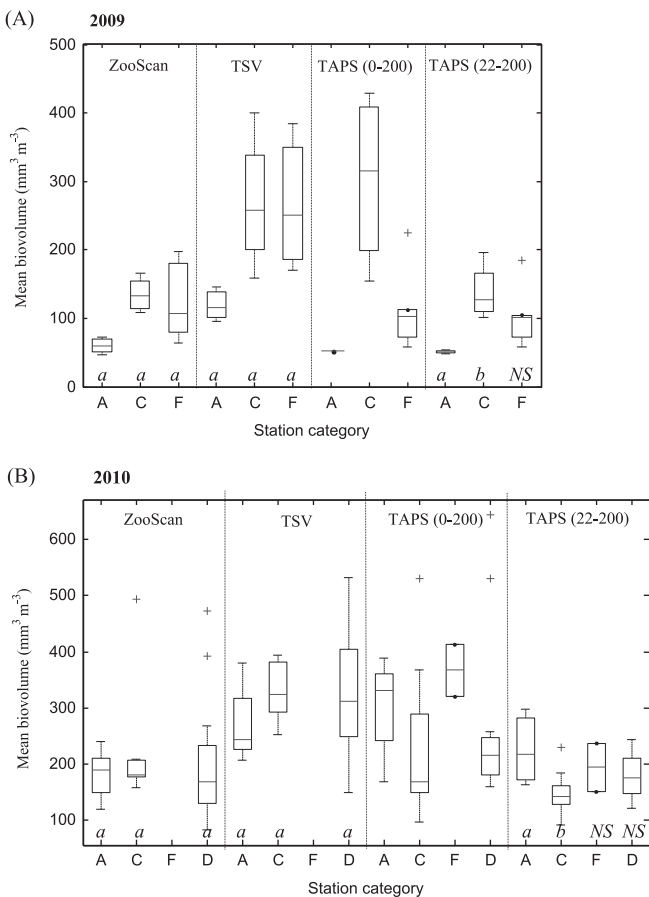

Fig. 7. Boxplots of mean biovolumes for the three methods during 2009 and 2010 for each mesoscale feature where *a* and *b* indicate significantly different means. A=anticyclone, C=cyclone, F=frontal, D=divergence.

for 2009, none of the differences between the structures were significant. For the TAPS 22–200 m results, the only significant difference ($p < 0.05$) was between the cyclonic and the anticyclonic mean biovolume (Fig. 7B).

In light of the variability of the hydrology observed within each of the features in 2010, data from the two dipoles were extracted and separated into cyclonic and anticyclonic categories (Fig. 8). The number of stations in each dipole structure was low, and therefore the ANOVA tests showed no significant differences for any of the methods, except Dipole 2 with the TAPS 22–200 m data

($p < 0.05$). There was also no significant difference when comparing each feature between the dipoles. For the TAPS results, the difference between the two dipoles clearly related to the surface layer that was abundant in zooplankton in the first dipole (Fig. 8). The difference between the ZooScan and TAPS 22–200 m data for the cyclonic feature of dipole 2 could be explained by the presence of stations C34 and C36, where the large sizes dominated the ZooScan biovolume (Fig. 5C).

The main differences between the two years with regard to size composition were as follows: (1) the contribution of the smallest size class was most important at cyclonic stations in 2009, especially at the surface, while this size class was abundant in all structures during 2010, including the surface layer (Fig. 9); and (2) mean biovolume at anticyclonic stations was richer for all size classes in 2010 compared to 2009. The patterns observed in Fig. 7A and b were broadly replicated at the level of each size class. Multiple comparison tests with ANOVA and Bonferroni adjustment were performed to compare features. In 2009, despite the observed patterns, the only significant differences ($p < 0.05$) were for the size class ESR > 1 mm for the TAPS 22–200 m data (A < C and F) and size class ESR < 0.2 mm for the ZooScan (A < C). In 2010, the size composition was more consistent between cyclonic, anticyclonic and divergence stations, but none of the differences were significant for the ZooScan data. For the TAPS 22–200 m data, the only significant difference was for the class ESR < 0.2 mm (A > C).

In terms of size composition, the ESR classes > 1 mm dominated biovolumes in 2009, but their weight was lower in cyclonic structures and the smaller sizes were more prevalent. In the anticyclones, the weight of large organisms was more dominant (Table 3, results for the common depth range TAPS 22–200 m). In 2010, the two legs were different as in leg 1 the proportion of small particles was particularly high at anticyclonic stations and low in the cyclones. During leg 2, the proportion of the third class (ESR 0.5–1 mm) increased relative to the others, becoming higher than the weight of the 0–0.2 mm class in all features.

Considering that shallow mixed layers were common and to complement the results on size composition, biovolume spectra were calculated from the TAPS 0–200 m data for each year and each feature (Fig. 10) using the methods of Zhou (2006) and Schultes and Lopes (2009). The log biovolume bins below ~ -1.5 corresponded to the 0–0.2 mm ESR class. Differences between the structures were mainly observed in this part of the spectrum in 2009 when the cyclonic features exhibited a much higher level in biovolume of small cells and a steeper slope. Anticyclonic and divergence structures were characterized by a lower slope and
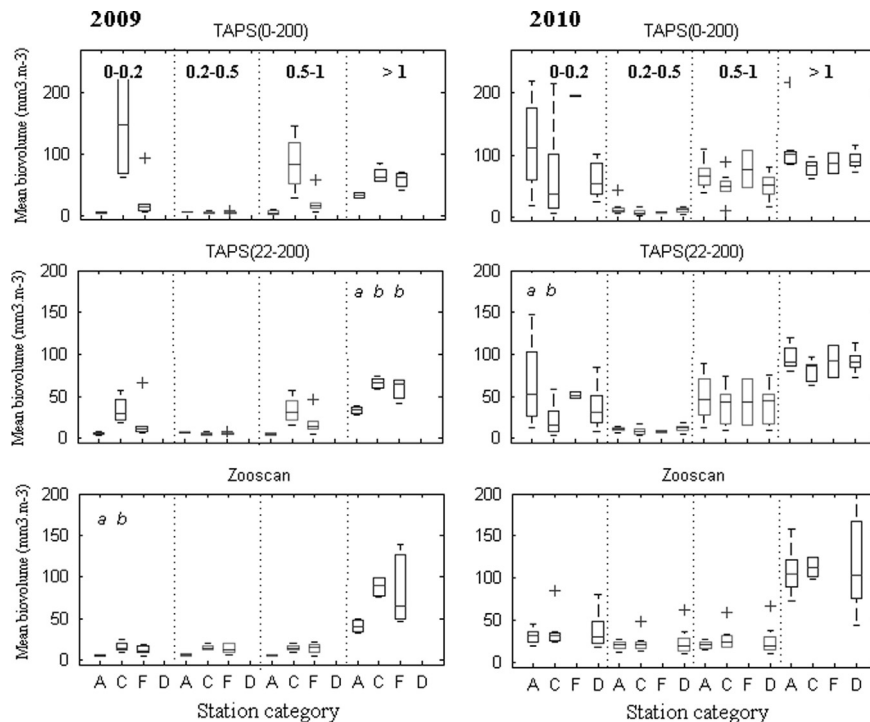
Fig. 9. Boxplots of mean biovolumes for each size class measured by the TAPS and the ZooScan, for each mesoscale feature for 2009 and 2010, where *a* and *b* indicate significantly different means. A=anticyclone, C=cyclone, F=frontal, D=divergence.

Table 3
Percentage contribution of each size class to mean biovolume in the water column from TAPS 22–200 m data.

Biovolume %	2009				2010 Leg 1				2010 Leg 2			
	0–0.2 mm	0.2–0.5 mm	0.5–1 mm	1–3 mm	0–0.2 mm	0.2–0.5 mm	0.5–1 mm	1–3 mm	0–0.2 mm	0.2–0.5 mm	0.5–1 mm	1–3 mm
Cyclone	24.5	3.7	24.2	47.6	16.6	8.4	19.0	56.0	13.6	3.6	30.4	52.4
Anticyclone	11.6	13.5	9.5	65.5	35.3	5.3	13.6	45.8	23.2	4.2	32.7	39.9
Divergence					24.0	9.1	10.4	56.5	20.1	5.1	27.8	47.1
Front	19.1	5.4	17.9	57.6	26.4	4.2	22.4	47.1				

similar spectra. Within the frontal stations, station 4 stands out, showing the same spectrum as the mean cyclonic spectrum (data not shown) and a similar slope (table in Fig. 10). There was less difference in biovolume between features for the additional larger peaks, except at ~0.4 on the *x*-axis (i.e. ESR ~0.84 mm) where there was a high peak for the cyclones. In 2010, the three biovolume spectra from leg 1 (Dipole 1) are remarkably similar, with only the anticyclone biovolume slightly higher than the two other features in the size range of the dome (ESR 0–0.13 mm). The additional larger peaks were usually of similar magnitude in all three features. The slope for the anticyclone was slightly steeper than those for the cyclone and the divergence. For leg 2 (Dipole 2), the points were more scattered, with lower overall biovolume, particularly for the cyclones in the small size range, and lower slopes for the anticyclonic and cyclonic features, with the steepest slope being observed for the divergence structures.

Correlations between abundance at stations and environmental conditions, expressed through parameters such as SLA, geostrophic velocity, depth of the mixed layer and chlorophyll characteristics are presented in Table 4. There was a strong negative correlation between biovolume and SLA in 2009 (total biovolume and for 3 of the 4 size classes) but not in 2010. There was no apparent relationship with geostrophic velocity and low correlation with chlorophyll characteristics (Table 4). A negative correlation was found between mixed layer depth and biovolume that

was highly significant in 2009 ($p \ll 0.001$), but only marginal in 2010 for the smaller size class with a lower significance ($p=0.047$).

3.3. Zooplankton vertical structure from acoustic data

The vertical distribution of biovolume obtained from TAPS profiling, together with hydrographic structure, is presented in Fig. 11 for selected sections through eddies, fronts and divergence zones. No clear vertical diurnal migration was observed at the stations in the Mozambique Channel (Fig. 12) and therefore a comparison of day–night patterns could not be undertaken. In 2009, high concentrations of zooplankton were observed in the mixed layer close to the surface at stations in the cyclone and at station 4. Although station 4 had a geostrophic velocity that categorized it as a frontal station, its characteristics were very similar to those of cyclonic stations (Fig. 11A). In the frontal area, the biovolume had a vertical distribution that was spread throughout the profiled water column, particularly for size class 4 (1–3 mm). Size classes 1 (0–0.2 mm) and 3 (0.5–1 mm) had similar distribution, with the pattern for class 3 being high biovolume at cyclonic stations and very low at the anticyclonic stations. Class 2 (0.2–0.5 mm) had low biovolume, especially at stations in the cyclonic feature, and was mainly present in the lower half of the mixed layer. The vertical distribution of class 4 was much greater than the other classes, especially at frontal stations. There was also
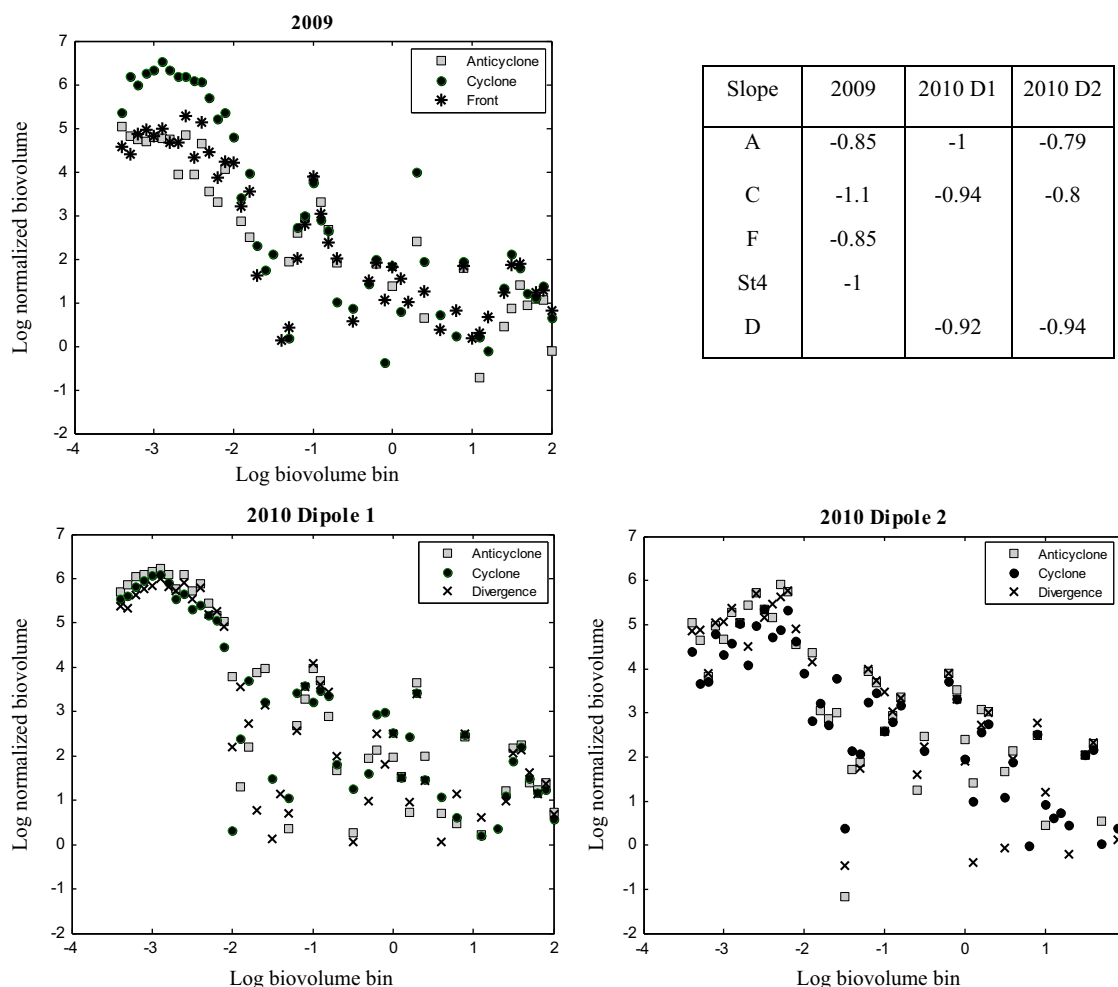
Slope	2009	2010 D1	2010 D2
A	-0.85	-1	-0.79
C	-1.1	-0.94	-0.8
F	-0.85		
St4	-1		
D		-0.92	-0.94

Fig. 10. Mean biovolume spectra for each mesoscale feature in 2009, and dipole 1 and dipole 2 in 2010. The slopes of the spectra for each feature are presented in the table. A=anticyclone, C=cyclone, F=frontal, D=divergence.

Table 4
Significant correlation coefficients ($^*p < 0.05$, $^\#p < 0.1$) between mean biovolume (0–200 m) and various environmental parameters. GV: geostrophic velocity.

	SLA	GV	Surface Chl	Maximum Chl	Integrated Chl	Depth of maximum Chl	Mixed layer depth
MC09B							
Total	− 0.73*	− 0.08	− 0.32	− 0.17	− 0.46	− 0.27	− 0.78*
0–0.2 mm	− 0.65*	− 0.13	− 0.21	− 0.19	− 0.38	− 0.23	− 0.71*
0.2–0.5 mm	0.42	− 0.24	0.41	0.57*	0.52$^\#$	0.14	0.46$^\#$
0.5–1 mm	− 0.67*	− 0.07	− 0.33	− 0.17	− 0.42	− 0.20	− 0.74*
> 1 mm	− 0.85*	0.22	− 0.65*	0.01	− 0.7*	− 0.48$^\#$	− 0.77*
MC10A							
Total	0.14	0.12	0.19	− 0.15	0.05	0.17	− 0.24
0–0.2 mm	0.01	0.13	0.26	− 0.06	0.08	− 0.02	− 0.34*
0.2–0.5 mm	0.17	− 0.1	0.20	− 0.2	− 0.05	0.28	0.04
0.5–1 mm	0.21	0.03	− 0.24	− 0.11	− 0.00	0.28	0.18
> 1 mm	0.41*	− 0.04	− 0.12	− 0.3$^\#$	− 0.08	0.59*	0.17

high zooplankton abundance at the bottom of the mixed layer in the cyclonic feature (Fig. 11A).

For 2010, data from the two legs are presented separately as these two periods show somewhat different results. Leg 1 displayed mainly very high near-surface concentrations in the cyclonic eddy of dipole 1, compared to low concentrations in the cyclone of dipole 2 during leg 2 (Fig. 11B). As in 2009, class 1 biovolumes were confined to the upper 50 m and class 2 was found more or less in the deeper half of the mixed layer. The class 3 pattern was similar to that of class 1 during leg 1, but was more deeply distributed during leg 2, while class 4 had extensive

vertical distribution during both legs, with maximum abundance at 50–100 m. The main difference between 2009 and 2010 was that these patterns did not show dependence on the mesoscale features. A significant observation for the cyclonic eddies in both years was that the peak concentrations of class 4 zooplankton (1–3 mm) coincided with the fluorescence maximum. It appeared that there was a similar coincidence for class 2 (0.2–0.5 mm), but to a lesser extent in 2009 (Fig. 12).

Fig. 13 shows the relationship between biovolume–temperature correlation coefficients and biovolume–salinity correlation coefficients for each size class and for stations categorized to each
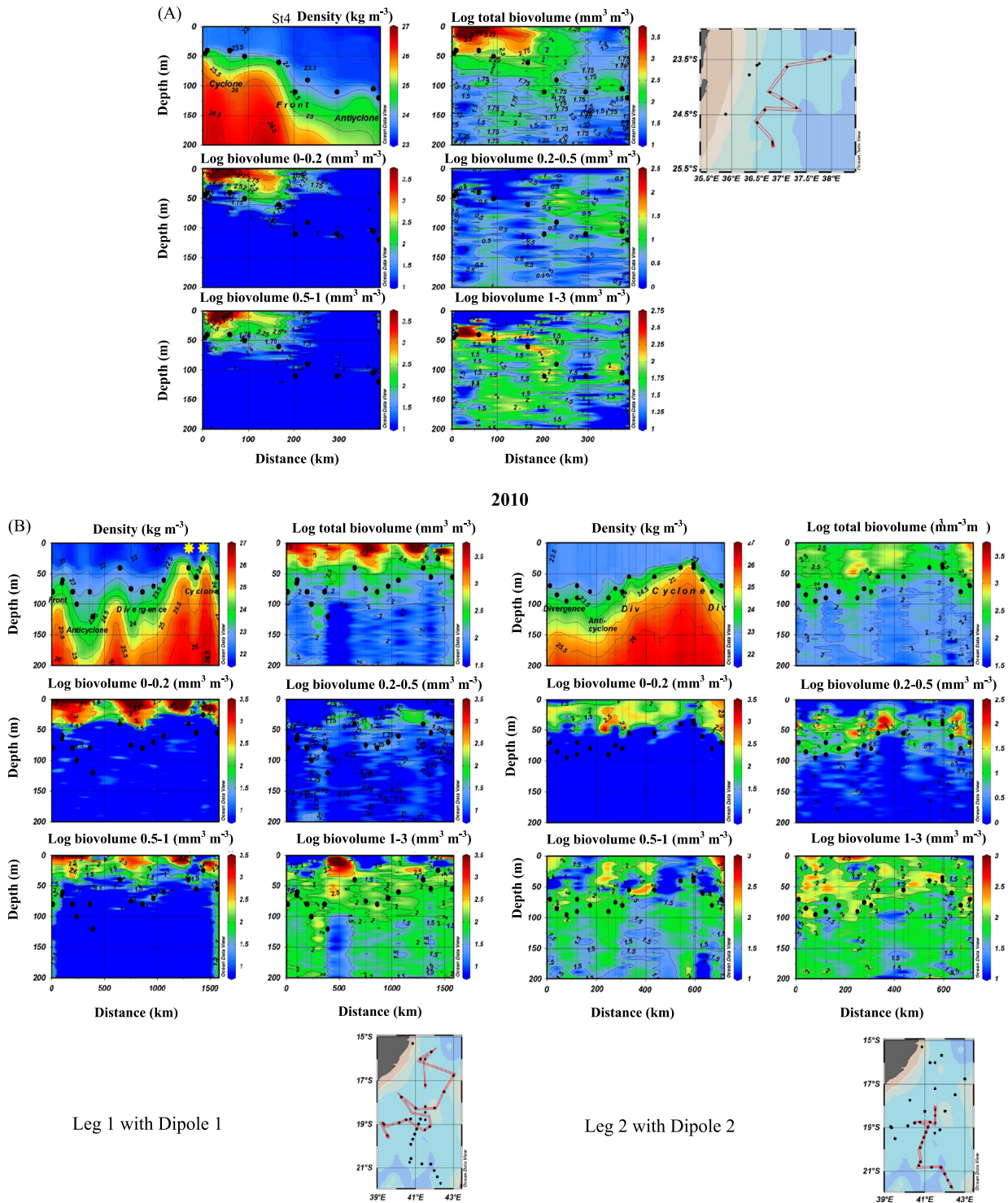
Fig. 11. Vertical patterns of density and $\log_{10}$ biovolume (total and size class) through selected sections of mesoscale features for (A) 2009 and (B) dipole 1 and dipole 2 in 2010. Black dots indicate the depth of the chlorophyll maximum. Relevant mesoscale features are indicated on the density plots. Sun symbols in (B) indicate two daytime cyclonic stations.

mesoscale feature. In 2009, cyclonic and anticyclonic stations were clearly separated for class 1 and also for class 3, but not for class 4. For classes 1 and 3, the correlations were positive and highly significant ($p < 0.01$). The correlations were weaker for class 2, being significant for anticyclonic stations ($p < 0.05$) but not significant for the cyclones. Frontal stations could not be easily distinguished from the other categories for any size class. For 2010, the smallest organisms (class 1) were well correlated with temperature for all the station categories (Fig. 13) but particularly

for cyclones. There were also good correlations of biovolume versus salinity for the cyclones, while frontal and divergence stations showed a large range in correlation coefficients for both temperature and salinity.

3.4. Taxonomic composition of the size classes

ZooScan analysis and image processing of Multinet samples yielded a total of 42 taxonomic or abiotic groups. The most abundant
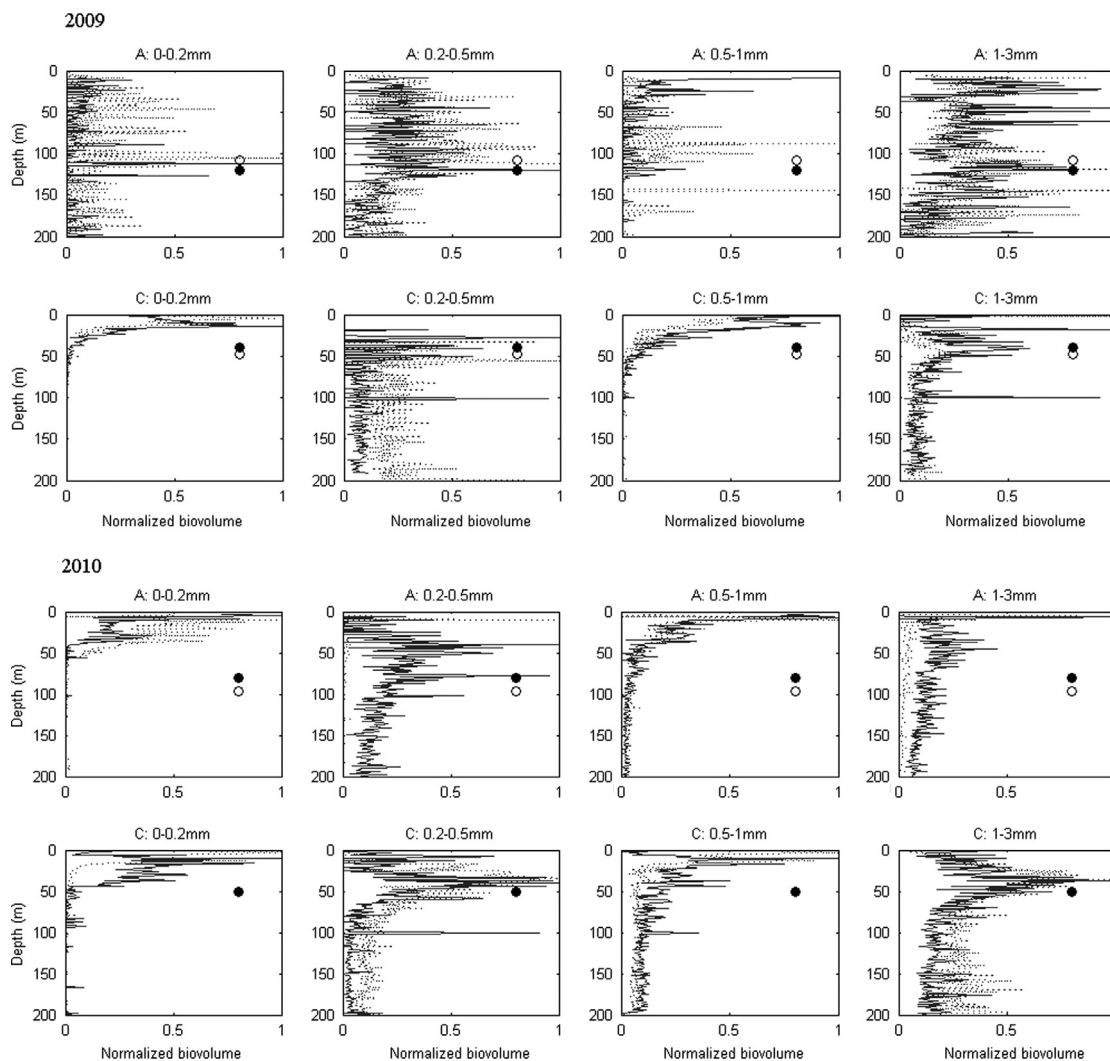
Fig. 12. Profiles of mean day and night normalized biovolume for each size class during 2009 and 2010, for cyclones (C) and anticyclones (A). The mean depths of the upper mixed layer for day and night are indicated.

and most commonly found organisms within the four TAPS size classes at representative cyclonic and anticyclonic stations for both cruises are shown in Fig. 14. The larger organisms (> 3.0 mm ESR) not sampled by TAPS but collected with the Multinet are also included. In total there were 28 taxonomic groups which includes one for 'detritus' (a grouping of an inseparable copepod–detritus matrix) and one for 'various meroplankton' (i.e. bivalve, brachiopod, cyphonaute, cirripede, echinoderm and gastropod larvae, as well as crab zoeae). Size class 1 (0.0–0.2 mm ESR) comprised mostly small copepods (calanoids, poecilostomatoids, cyclopoids), detritus and ostracods at both cyclonic and anticyclonic stations during both cruises, as well as some dinoflagellates (likely *Pyrocystis* sp.) and foraminiferans (likely *Globigerina* sp.) at the cyclonic stations in 2009. Size class 2 (0.2–0.5 mm ESR) comprised mainly calanoid copepods and detritus, with low quantities of ostracods, small chaetognaths and appendicularians. The 0.5–1.0 mm ESR size class 3 had a similar taxonomic composition except that the proportion of chaetognaths at most stations was higher. Size class 4 (1.0–3.0 mm ESR) comprised mainly large calanoid copepods and chaetognaths, with considerably more detritus during 2010, gelatinous zooplankton (e.g. siphonophores, salps), and euphausiid furcilia. The largest size class 5 (> 3.0 mm ESR) comprised mainly large chaetognaths, gelatinous zooplankton (siphonophores, salps, hydromedusae, ctenophores), large calanoid copepods, detritus (or copepod-detritus

matrices), and larger crustaceans such as euphausiids (especially at night) and decapod larvae.

The taxonomic composition of the dominant zooplankton determined by the ZooScan method (which is only applicable to broad taxonomic groupings) did not vary greatly between cyclonic and anticyclonic stations, or at frontal and divergence stations (data not shown). There was also an absence of strong clustering of the functional groups amongst the four TAPS size classes, as all classes were dominated by herbivorous or omnivorous calanoid copepods. Some carnivorous species were found in all size classes. The increased proportion of gelatinous zooplankton in the larger size classes included both herbivorous (salps, doliolids, appendicularians) and predatory (siphonophores, hydromedusae) species. The proportion of detritus was greater during 2010, as was the proportion of biovolume attributed to the copepod/detritus matrix, which was sticky and difficult to separate.

4. Discussion

4.1. Methods comparison

Mean biovolumes from TSV measurements on the Multinet samples were consistently greater than those estimated by both
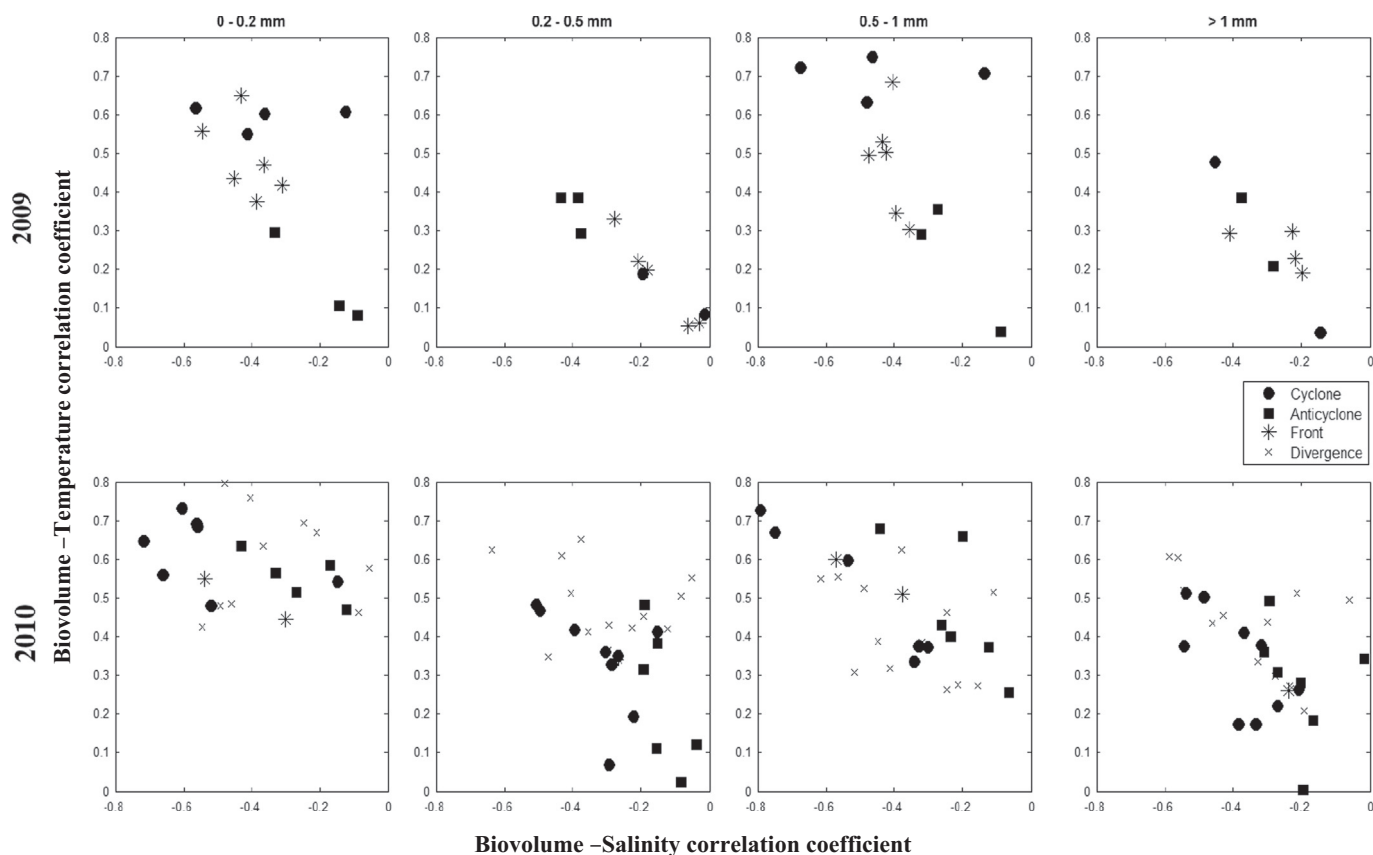
Fig. 13. Relationships between biovolume–temperature correlation coefficients and biovolume–salinity correlation coefficients for each size class and stations categorized according to mesoscale features, for 2009 and 2010.

the ZooScan and TAPS. This is due to measurements from the TSV method tending to overestimate true biovolume due to water being trapped interstitially between organisms. Multinet-derived settled biovolume generally exceeds the more accurate biovolume measurements of the ZooScan, which are based on the dimensions of each scanned object. A second factor is that the Multinet is able to sample much larger organisms than the TAPS, although it must be borne in mind that the 200 μm mesh size results in under sampling of the smallest size class relative to the TAPS (effectively 0.05–0.2 mm ESR, equivalent to 100–400 μm ESD, Gallienne and Robins, 2001). As the largest size fraction sampled by the Multinet (>3 mm ESR) consistently comprised the greatest proportion of the TSV, and the largest size fraction sampled by TAPS (>1 mm ESR) consistently comprised the greatest proportion of total TAPS biovolume (Table 4), it can deduced that the TSV will consistently represent the most biovolume, even accounting for high concentrations of particles too small to be retained by the 200 μm mesh. In some situations with particularly high concentrations of the smallest sized organisms very close to the surface, the TAPS (0–200 m) and TSV results were similar, as in 2009 for the cyclonic eddy and in 2010 for the anticyclone (Fig. 7).

Another important consideration is that the ZooScan is suitable only for analysis of organisms >150 μm ESR as it has a pixel resolution of 10.6 μm (Gorsky et al., 2010). Despite this technical limitation, generally differences between the TAPS and ZooScan results were minor, except when the 0–0.2 mm class dominated the composition (e.g. cyclonic stations in 2009 and most features in 2010, Fig. 7). Additionally, the processing in each method determines its own spherical radius with uncertainties. For the acoustics, the algorithm leads to the most probable population fitting the measured data. For the optical method, the position and view angle influences the calculated diameter. Some shifts may

have occurred between the 0–0.2 and 0.2–0.5 mm size classes on the one hand, and between the 0.2–0.5 and 0.5–1 mm classes on the other hand (Fig. 9).

Overall the three methods showed consistency between the two years (Fig. 6), with higher biovolumes in 2010 than in 2009. The more detailed comparison according to mesoscale features (Figs. 7 and 8) showed good coherence between features in 2009 but not in 2010. All three methods were expected to mainly characterize the mesozooplankton, but as noted previously, each method is more favorable for a particular size fraction of the population. Generally, though, the methods were complementary.

Vertical profiling with TAPS provides fine scale resolution of the vertical distribution of particles in different size classes that cannot be obtained with conventional net sampling. Conversely, both microscopic and imaging analysis yields information on the taxonomic composition of organisms in the water column that cannot be inferred from acoustic data, and are also able to assess larger sizes. The ZooScan method is a step closer to taxonomic identification of the community, obviating tedious detailed microscope identification. The fine scale vertical resolution which is possible with the TAPS provides profile data that can be compared with environmental parameters.

4.2. Yearly and mesoscale feature impacts on zooplankton distribution and composition

The apparent variability in the ecosystem between 2009 and 2010 was possibly related to the prevailing eddy fields during these 2 years. In 2009, a well defined dipole was sampled that had formed approximately 2 months prior to the cruise and remained quasi-stationary during the sampling period (Ternon et al., 2014). In contrast, the eddy field in 2010 was more extensive and largely
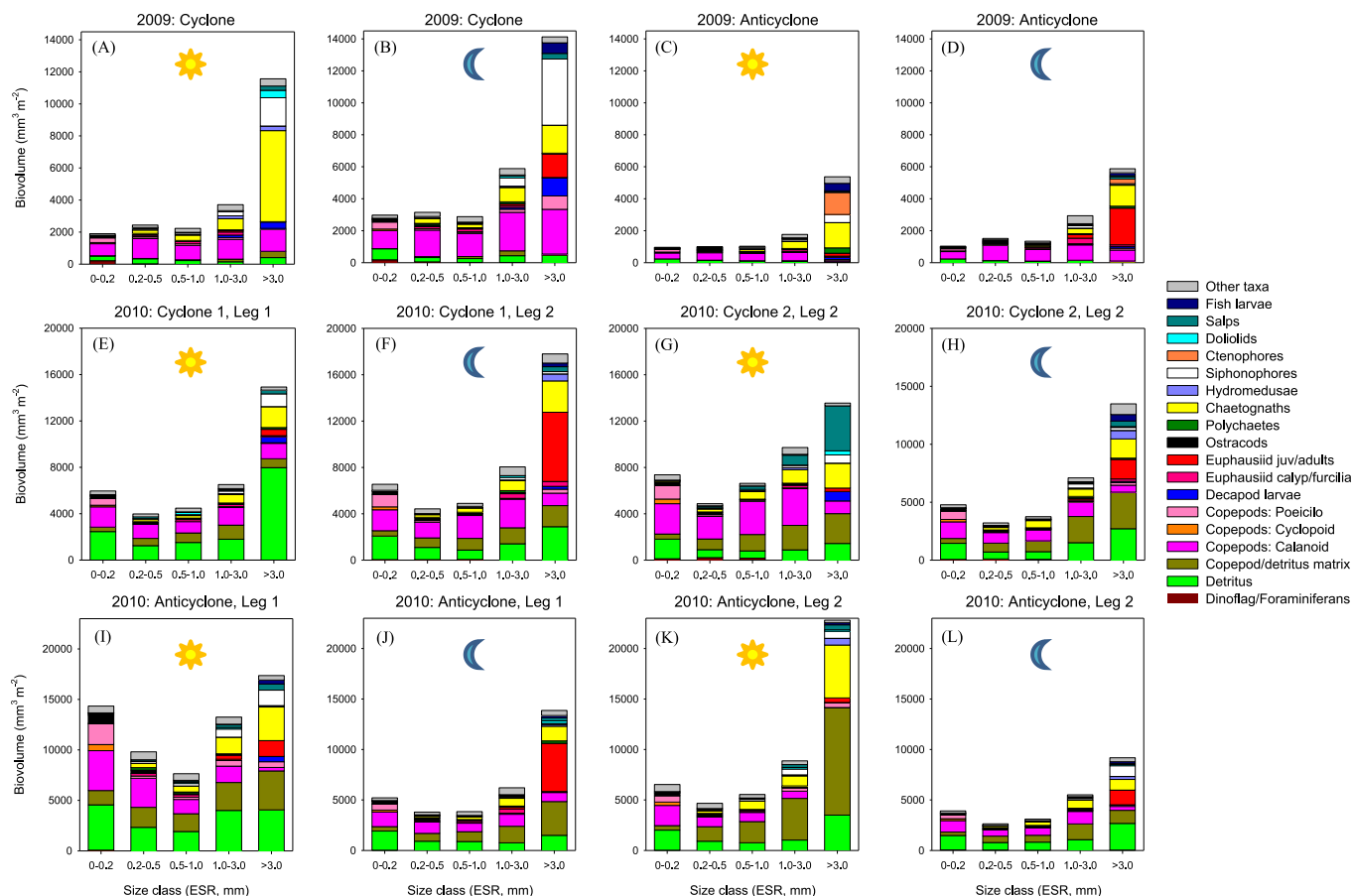
Fig. 14. Composition of zooplankton populations (biovolume) in five size classes for representative stations from cyclones and anticyclones in 2009 and 2010, during the day (sun) and night (moon). Examples for leg 1 and leg 2 in 2010 are shown separately, with cyclone 1 located in the north and cyclone 2 in the south (Fig. 1A).

unstable (i.e. eddies moving, disappearing and merging). The most consistent feature was the well developed cyclonic eddy in the narrows of the Mozambique Channel (15–18°S) that remained stable during both legs of the cruise (Lamont et al., 2014, their Fig. 5A–D). The large anticyclonic eddy sampled during leg 1 shifted westwards midway through the cruise and then merged with a smaller anticyclonic eddy moving southwards near the Mozambique shelf (Ternon et al., 2014). Consequently, the "anticyclonic" stations sampled during leg 2 were located in the rapidly retreating and dissipating eastern perimeter of the eddy. Also, the cyclonic eddy situated farther south (20–21°S) that was sampled during leg 2 was newly formed with a comparatively weak SLA (Lamont et al., 2014).

4.2.1. Global results

The results obtained in 2009 indicated the same trend between features for all methods, demonstrating higher concentrations of zooplankton in the cyclones compared to the anticyclones. This is consistent with the mechanism of cool, nutrient-rich water upwelling in the core of the cyclonic eddy enriching the surface layers in oligotrophic environments (McGillicuddy et al., 1998; Oschlies and Garçon, 1998; Zimmerman and Biggs, 1999). The same observations have been made during this study with respect to total chlorophyll *a* concentrations at the surface by Barlow et al. (2014) and also for higher trophic levels such as the micronekton concentration (Béhagle et al., 2014). In 2010, the difference in zooplankton biovolume between cyclonic and anticyclonic stations was smaller than in 2009, but it is important to note that this difference varied depending on the method used to determine

biovolume. We have demonstrated that despite the high overlap in their sampling ranges, each method is better suited for a particular size range of organisms. Interestingly, a coupled biogeochemical model PISCES with the regional oceanic model ROMS has produced results that are in contrast with previous studies in the open ocean, where relatively low chlorophyll concentrations were found in the core of cyclonic eddies and higher chlorophyll concentrations in anticyclonic eddies (José et al., 2014). Béhagle et al. (2014) also found that, depending on the acoustic frequency considered, either the cyclonic or anticyclonic eddies can yield the higher mean abundance of organisms. This is dependent on the type and size of the organisms considered, however. The particular eddy field structure in 2010, coupled with a possible eddy-shelf interaction and offshore transport of coastal production, resulted in observations that were different to those obtained in the open ocean (José et al., 2014; Kolasinski et al., 2012; Ternon et al., 2014).

Although the two cruises were conducted during different seasons, austral summer in 2009 and late autumn–winter in 2010, no relationship was found between zooplankton abundance and surface chlorophyll *a* concentration. Other studies in the Mozambique Channel demonstrated that surface chlorophyll *a* was maximal in winter (July) and minimal in summer (December) (Levy et al., 2007). Tew-Kai and Marsac, 2009 observed higher concentrations of phytoplankton in cyclones compared to anticyclones, as was found in 2009 (Barlow et al., 2014) but not in 2010 when both features had similar concentrations. Tew-Kai and Marsac (2009) also noted that surface phytoplankton in the central part of the Channel was constrained more by mesoscale activity than by seasonality. Zooplankton biovolume was found to be elevated in all mesoscale features in 2010, resulting in the overall

biovolume being greater than in 2009, when higher biovolume was mostly observed in cyclones and to a lesser extent at frontal stations.

4.2.2. Relationships with environment

The influence of the SLA and upper mixed layer on zooplankton abundance was demonstrated in 2009 by the negative correlations with mean biovolume over a depth of 200 m. This is related to the consistency of the hydrological structure for each group of stations that were categorized according to the eddy field features. It should be noted that station 4 was classified as a frontal station because it had high geostrophic velocity (Lamont et al., 2014) but no relationship was established between geostrophic velocity and the zooplankton biovolume (Table 4). In fact, the hydrology of station 4 was very similar to cyclonic stations with shallow mixed layers and, consequently, the zooplankton composition and spatial distribution of size classes were similar.

In 2010, two different cyclonic structures were studied, with each cyclone having a different evolutionary history (Ternon et al., 2014). The northern, stable cyclone at ~16°S was sampled during leg 1, whilst the cyclone at ~21°S, sampled during leg 2, was newly established and in the process of splitting (Ternon et al., 2014). The SLA associated with the northern cyclone was greater than the southern cyclone, and the shallow mixed layer combined with the stability seemingly provided favorable conditions for particle accumulation at the surface (Fig. 11B, black arrows). In contrast, there were apparently no clear enrichment phenomena in the newly established cyclone in the south, and the vertical distribution of zooplankton appeared to be strongly constrained by the density gradient in the water column (Fig. 11B). Mixed layer depth and SLA were not correlated with zooplankton abundance, but the correlation between biovolume and temperature was significant for all eddy features, being particularly high for the smallest size class. However, the characteristic of being either "cyclonic" or "anticyclonic" may not be the determining factor in complex ecosystems, as noted by Godø et al. (2012), who discussed the overall increase in marine life within mesoscale eddies in general.

4.2.3. Size composition

The nature of particles too small to be sampled by the Multinet but recorded by the TAPS can only be speculated upon, as no water samples for the $< 200\,\mu m$ size range (equivalent to < 0.1 mm ESR, or < 0.2 mm ESD) were collected. Possible candidates for this size range include diatoms, microzooplankton and marine aggregates or "marine snow". Diatoms were unlikely to be responsible for the high concentrations of small particles (< 0.1 mm ESR) detected by the TAPS in the 2009 cyclonic eddy since there was no corresponding peak in chlorophyll a. In contrast, chlorophyll concentrations were twice as high at the surface in the anticyclonic eddy and slightly higher at the depth of the fluorescence maximum. Marine snow may include living or dead material such as diatoms, fecal pellets, discarded zooplankton feeding structures and general detritus (Jackson and Burd, 1998). González-Quirós and Checkley (2006) inferred that particles detected by an optical plankton counter (OPC), but not collected by net, were likely to be fragile particles such as aggregates and abandoned appendicularian houses. Their sampling was conducted in the California upwelling region where particles were found to be > 1.26 mm ESD (González-Quirós and Checkley, 2006) and 0.4–0.8 mm ESD (median) (Jackson and Checkley, 2011), and therefore considerably larger than the unidentified small particles in this study. Furthermore, the marine snow in California was observed to be maximum at 15–70 m (Jackson and Checkley, 2011), unlike the near-surface (0–20 m) maxima observed in this study. Nevertheless, the presence of appendicularians in all size classes means that marine snow may possibly be present in the Mozambique Channel.

It is more likely that these small particles comprised micro-zooplankton (protozooplankton), comprising tintinnids, ciliates, heterotrophic dinoflagellates and metazoans such as juvenile stages of small copepods. Hopcroft et al. (2001) noted that over half to one quarter of copepod biomass in tropical waters is not sampled by a 200 μm net, where missing components comprise largely nauplii and small copepodites. No data are available on microzooplankton abundance in the southwest Indian Ocean (SWIO), but Edwards et al. (1999) reported an average abundance of 3200 cells l^{-1} in oligotrophic waters of the Arabian Sea and up to 16,000 cells l^{-1} in upwelled waters. Arabian Sea microzooplankton was dominated by ciliated protozoa, mostly aloricate oligotrichs and choreotrichs, while the metazoan component comprised copepod nauplii and small appendicularians. Stelfox et al. (1999) found average standing stocks of microzooplankton (~ 100 mg C m^{-2}) to be similar to those of mesozooplankton in oligotrophic areas of the Arabian Sea, and a third of mesozooplankton standing stocks in more nutrient rich waters, indicating the potential importance of microzooplankton in the Indian Ocean. It is also likely that microzooplankton abundance maybe enhanced in higher nutrient waters such as those resulting from upwelling in the core of a cyclonic eddy. The highest concentrations of small particles during this study were found in the 2009 cyclonic eddy, but elevated microzooplankton was also observed near the surface at two cyclonic stations in 2010 (Fig. 11B, sun symbols) as well as in other mesoscale features.

To our knowledge, this is the first time that biomass spectra have been applied to acoustic data, represented here as biovolume spectra (Fig. 10). The size classes considered in this study were much smaller than those usually obtained from nets, OPC (Zhou, 2006) or LOPC (Schultes and Lopes, 2009), but general biomass spectrum theory can be applied to bacteria, phytoplankton, zooplankton and even larger organisms (Zhou, 2006). From these first observations, the slopes are close to -1 for the most stable features and decrease (in absolute value) for less stable structures such as dipole 2 in 2010 (Fig. 10). The slopes obtained by means of acoustic data were steeper than those obtained by means of the net and ZooScan processing (J. Huggett, unpublished data), caused by the high biovolumes of the very small size class at the beginning of the spectrum. The slopes in Fig. 10 are values for the entire biovolume bin range, but within sections of the spectra are positive and negative slopes that may depict the compensation between growth rates within biovolume bin intervals and the losses due to sinking and mortality (Zhou and Huntley, 1997).

Differences in biovolume distribution according to mesoscale feature, size and depth were mainly the result of higher or lower concentrations of the same community structure, with larger organisms tending to be located deeper in the water column due to their greater diel migration ability. Similar species composition was observed in cyclonic and anticyclonic eddies in the Mozambique Channel during 2007 and 2008 (Huggett, 2014) as has also been noted off Hawaii (Landry et al., 2008) and Western Australia (Strzelecki et al., 2007). What is evident from the TAPS data is the abundance of organisms of size classes 0.2–0.5 mm and > 1 mm ESR in the vicinity of the chlorophyll maximum, especially at cyclonic stations. This is difficult to interpret, however, given the similarity in community composition in all mesoscale features. The two smallest classes were dominated by copepods of all feeding modes, but the smallest class was confined to the upper mixed layer. There were mainly herbivorous/omnivorous organisms (copepods, euphausiids, salps) in the largest TAPS size class but these were also mixed with some carnivorous taxa (chaetognaths, siphonophores). This suggests there may be two separate communities. One is concentrated in the

upper mixed layer, dominated by the smallest size fraction (0–0.2 mm ESR), and comprising mainly microzooplankton and very small copepods feeding on small particles. The other community comprises larger organisms (>0.2 mm ESR) at the depth of the chlorophyll maximum where there is an adequate food supply for herbivorous zooplankton.

In conclusion, the methodological comparison showed (1) that biovolume of the Multinet samples was consistently overestimated by TSV compared to the TAPS and ZooScan estimates, (2) that TAPS was a better estimator of small (<0.2 mm) particles, and (3) the Multinet/ZooScan was a better estimator of large (>3 mm) particles. The methods were consistent, however, in demonstrating that overall, higher zooplankton biovolume was associated with cyclonic eddies compared to anticyclonic eddies under stable mesoscale conditions, such as for the well established dipole in 2009. The same trend was observed for the stable northern cyclone in 2010 but with less evidence. The three methods tended to give conflicting results for unstable mesoscale conditions, typified by the weak southern cyclone and dissipating anticyclonic eddies in 2010, because of the greater differences in size composition of these evolving or dispersing mesoscale features, and the different size bias for each method.

Acknowledgments

References

Backeberg, B.C., Reason, C.J.C., 2010. A connection between the South Equatorial Current north of Madagascar and Mozambique Channel Eddies. Geophys. Res. Lett. 37, L04604, http://dx.doi.org/10.1029/2009GL041950.

Bakun, A., 2006. Fronts and eddies as key structures in the habitat of marine fish larvae: opportunity, adaptive response and competitive advantage. Sci. Mar. 70 (S2), 105–122.

Barlow, R., Lamont, T., Morris, T., Sessions, H., van den Berg, M., 2014. Adaptation of phytoplankton communities to mesoscale eddies in the Mozambique Channel. Deep-Sea Res. II 100, 106–118.

Béhagle, N., du Buisson, L., Josse, E., Lebourges-Dhaussy, A., Roudaut, G., Ménard, F., 2014. Mesoscale features and micronekton in the Mozambique Channel: an acoustic approach. Deep-Sea Res. II 100, 164–173.

Capet, X., McWilliams, J.C., Molemaker, M.J., Shchepetkin, A.F., 2008. Mesoscale to submesoscale transition in the California Current System. Part I: Flow structure, eddy flux, and observational tests. J. Phys. Oceanogr. 38, 29–43.

Costello, J.H., Pieper, R.E., Holliday, D.V., 1989. Comparison of acoustic and pump sampling techniques for the analysis of zooplankton distributions. J. Plankton Res. 11, 703–709.

de Ruijter, W.P.M., Ridderinkhof, H., Lutjeharms, J.R.E., Schouten, M.W., Veth, C., 2002. Observations of the flow in the Mozambique Channel. Geophys. Res. Lett. 29, 1502, http://dx.doi.org/10.1029/2001GL013714.

Drazen, J.C., De Forest, L.G., Domokos, R., 2001. Micronekton abundance and biomass in Hawaiian waters as influenced by seamounts, eddies, and the moon. Deep-Sea Res. I 58, 557–566.

Edwards, E.S., Burkill, P.H., Stelfox, C.E., 1999. Zooplankton herbivory in the Arabian Sea during and after the SW monsoon, 1994. Deep-Sea Res. II 46, 843–863.

Falkowski, P.G., Ziemann, D., Kolber, Z., Bienfang, P.K., 1991. Role of eddy pumping in enhancing primary production in the ocean. Nature 352, 55–58.

Gallienne, C.P., Robins, D.B., 2001. Is *Oithona* the most important copepod in the world's oceans? J. Plankton Res. 23, 1421–1432.

Godø, O.R., Samuelsen, A., Macaulay, G.J., Patel, R., Hjøllo, S.S., Horne, J., Kaartvedt, S., Johannessen, J.A., 2012. Mesoscale eddies are oases for higher trophic marine life. PLoS ONE 7, e30161, http://dx.doi.org/10.1371/journal.pone.0030161.

González-Quirós, R., Checkley Jr., D.M., 2006. Occurrence of fragile particles inferred from optical plankton counters used in situ and to analyze net samples collected simultaneously. J. Geophys. Res. 111, C05S06, http://dx.doi.org/10.1029/2005JC003084.

Gorsky, G., Ohman, M.D., Picheral, M., Gasparini, S., Stemmann, L., Romagnan, J.-B., Cawood, A., Pesant, S., Garcia-Comas, C., Prejger, F., 2010. Digital zooplankton image analysis using the ZooScan integrated system. J. Plankton Res. 32, 285–303.

Greenlaw, C.F., 1979. Acoustical estimation of zooplankton populations. Limnol. Oceanogr. 24, 226–242.

Greenlaw, C.F., Johnson, R.K., 1982. Physical and acoustical properties of zooplankton. J. Acoust. Soc. Am. 72, 1706–1710.

Greenlaw, C.F., Johnson, R.K., 1983. Multiple frequency acoustical estimation. Biol. Oceanogr. 2, 227–252.

Gruber, N., Lachkar, Z., Frenzel, H., Marchesiello, P., Münnich, M., McWilliams, J.C., Nagai, T., Plattner, G.K., 2011. Eddy-induced reduction of biological production in eastern boundary upwelling systems. Nat. Geosci. 4, 787–792.

Hagen, W., 2000. 4.3 Biovolume and biomass determinations. In: Harris, R.P., Wiebe, P.H., Lenz, J., Skjoldal, H.R., Huntley, M. (Eds.), ICES Zooplankton Methodology Manual. Elsevier Academic Press, London, pp. 87–147.

Holliday, D.V., 1977a. Extracting bio-physical information from acoustic signatures of marine organisms. In: Andersen, N.R., Zahuranec, B.J. (Eds.), Oceanic Sound Scattering Prediction. Plenum Press, New York, pp. 619–624.

Holliday, D.V., 1977b. The use of swimbladder resonance in the sizing of schooled pelagic fish. Rapp. P.-v. Réun. Cons. Int. Explor. Mer. 170, 130–135.

Holliday, D.V., 1985. Active acoustic characteristics of nekton. In: Foerster, J.W. (Ed.), Biology and Target Acoustics of Marine Life. US Naval Academy, Annapolis, MD, pp. 115–154.

Holliday, D.V., 1992. Zooplankton acoustics. In: Desai, B.N. (Ed.), Oceanography of the Indian Ocean. Oxford-IBH, New Delhi, pp. 733–740.

Holliday, D.V., Pieper, R.E., 1980. Volume scattering strengths and zooplankton distributions at acoustic frequencies between 0.5 and 3 MHz. J. Acoust. Soc. Am. 67, 135–146.

Holliday, D.V., Pieper, R.E., 1995. Bioacoustical oceanography at high frequencies. ICES J. Mar. Sci. 52, 279–296.

Holliday, D.V., Pieper, R.E., Kleppel, G.S., 1989. Determination of zooplankton size and distribution with multifrequency acoustic technology. ICES J. Mar. Sci. 46, 52–61.

Hopcroft, R.R., Roff, J.C., Chavez, F.C., 2001. Size paradigms in copepod communities: a re-examination. Hydrobiology 453–454, 133–141.

Huggett, J., 2014. Mesoscale distribution and community composition of zooplankton in the Mozambique Channel. Deep-Sea Res. II 100, 119–135.

Jackson, G.A., Burd, A.B., 1998. Aggregation in the marine environment. Environ. Sci. Technol. 32, 2805–2814.

Jackson, G.A., Checkley Jr, D.M., 2011. Particle size distributions in the upper 100 m water column and their implications for animal feeding in the plankton. Deep-Sea Res. I 58, 283–297.

José, Y.S., Aumont, O., Machu, E., Penven, P., Moloney, C.L., Maury, O., 2014. Influence of mesoscale eddies on biological production in the Mozambique Channel: Several contrasted examples from a coupled ocean-biogeochemistry Model. Deep-Sea Res. II 100, 79–93.

Kalish, J.M., Greenlaw, C.F., Pearcy, W.G., Holliday, D.V., 1986. The biological and acoustical structure of sound scattering layers off Oregon. Deep-Sea Res. 33, 631–653.

Kolasinski, J., Kaehler, S., Jacquemet, S., 2012. Distribution and sources of particulate organic matter in a mesoscale eddy dipole in the Mozambique Channel (southwestern Indian Ocean): insight from C and N stable isotopes. J. Mar. Syst. 96–97, 122–131.

Lamont, T., Barlow, R., Morris, T., van den Berg, M., 2014. Characterisation of mesoscale features and phytoplankton variability in the Mozambique Channel. Deep-Sea Res. II 100, 94–105.

Landry, M.R., Decima, M., Simmons, M., Hannides, C.C.S., Daniels, E., 2008. Mesozooplankton biomass and grazing responses to Cyclone *Opal*, a subtropical mesoscale eddy. Deep-Sea Res. II 55, 1378–1388.

Lawson, C.L., Hanson, R.J., 1974. Solving Least Squares Problems. Prentice-Hall New Jersey.

Lebourges-Dhaussy, A., Coetzee, J., Hutchings, L., Roudaut, G., Nieuwenhuys, C., 2009. Zooplankton spatial distribution along the South African coast studied by multifrequency acoustics, and its relationships with environmental parameters and anchovy distribution. ICES J. Mar. Sci. 66, 1055–1062.

Levy, M., Shankar, D., Andre, J.-M., Shenoi, S., Durand, F., de Boyer Montegut, C., 2007. Basin-wide seasonal evolution of the Indian Ocean's phytoplankton blooms. J. Geophys. Res. 112, C12014.

Machu, E., 2000. Etude de l'interaction des processus physiques et biologiques dans le système du Courant des Aiguilles au sud de l'Afrique: Apport des observations spatiales, Thèse de Doctorat de l'Université Paul Sabatier Toulouse III.

McGillicuddy Jr., D.J., Robinson, A.R., Siegel, H.W., Jannasch, H.W., Johnson, R., Dickey, T.D., McNeil, J., Michaels, A.F., Knap, A.J., 1998. Influence of mesoscale eddies on new production in the Sargasso Sea. Nature 394, 263–266.

Muhling, B.A., Beckley, L.E., Olivar, M.P., 2007. Ichthyoplankton assemblage structure in two meso-scale Leeuwin Current eddies, eastern Indian Ocean. Deep-Sea Res. II 54, 1113–1128.

Napp, J.M., Ortner, P.B., Pieper, R.E., Holliday, D.V., 1993. Biovolume-size spectra of epipelagic zooplankton using a Multifrequency Acoustic Profiling System (MAPS). Deep-Sea Res. 40, 445–459.

Oschlies, A., Garçon, V., 1998. Eddy-induced enhancement of primary production in a model of the North Atlantic Ocean. Nature 394, 266–269.

Paterson, H.L., Knott, B., Waite, A.M., 2007. Microzooplankton community structure and grazing on phytoplankton, in an eddy pair in the Indian Ocean off Western Australia. Deep-Sea Res. II 54, 1076–1093.

Pieper, R.E., Holliday, D.V., Kleppel, G.S., 1990. Quantitative zooplankton distributions from multifrequency acoustics. J. Plankton Res. 12, 433–441.

Pieper, R.E., McGehee, D.E., Greenlaw, C.F., Holliday, D.V., 2001. Acoustically measured seasonal patterns of Zooplankton in the Arabian Sea. Deep-Sea Res. II 48, 1325–1343.

Quartly, G.D., Srokosz, M.A., 2004. Eddies in the southern Mozambique Channel. Deep-Sea Res. II 51, 69–83.

Sabarros, P.S., Ménard, F., Lévénez, J.-J., Tew-Kai, E., Ternon, J.-F., 2009. Mesoscale eddies influence distribution and aggregation patterns of micronekton in the Mozambique Channel. Mar. Ecol. Prog. Ser. 395, 101–107.

Schouten, M.W., de Ruijter, W.P.M., van Leeuwen, P.J., Ridderinkhof, H., 2003. Eddies and variability in the Mozambique Channel. Deep-Sea Res. II 50, 1987–2003.

Schultes, S., Lopes, R., 2009. Laser Optical Plankton Counter and Zooscan intercomparison in tropical and subtropical marine ecosystems. Limnol. Oceanogr. Methods 7, 771–784.

Seki, M.P., Polovina, J.P., Brainard, R.E., 2001. Biological enhancement at cyclonic eddies tracked with GEOS thermal imagery in Hawaiian waters. Geophys. Res. Lett. 28, 1583–1586.

Stelfox, C.E., Burkill, P.H., Edwards, E.S., Harris, R.P., Sleigh, M.A., 1999. The structure of zooplankton communities, in the 2 to 2000 μm size range, in the Arabian Sea during and after the SW monsoon, 1994. Deep-Sea Res. II 46, 815–842.

Strzelecki, J., Koslowa, J.A., Waite, A., 2007. Comparison of mesozooplankton communities from a pair of warm- and cold-core eddies off the coast of Western Australia. Deep-Sea Res. II 54, 1103–1112.

Ternon, J.F., Roberts, M.R., Morris, T., Hancke, L., Backeberg, B., 2014. In situ measured current structures of the eddy field in the Mozambique Channel. Deep-Sea Res. II 100, 10–26.

Tew-Kai, E., Marsac, F., 2009. Patterns of variability of sea surface chlorophyll in the Mozambique Channel: a quantitative approach. J. Mar. Syst 77, 77–88.

Tew-Kai, E., Marsac, F., 2010. Influence of mesoscale eddies on spatial structuring of top predators' communities in the Mozambique Channel. Prog. Oceanogr. 86, 214–223.

Yebra, L, Almeida, C., Hernández-León, S., 2005. Vertical distribution of zooplankton and active flux across an anticyclonic eddy in the Canary Island waters. Deep-Sea Res. I 52, 69–83.

Weimerskirch, H., Le Corre, M, Jaquemet, S., Potier, M., Marsac, F., 2004. Foraging strategy of a top predator in tropical waters: great frigate birds in the Mozambique Channel. Mar. Ecol. Prog. Ser. 275, 297–308.

Zhou, M., 2006. What determines the slope of a plankton biomass spectrum? J. Plankton Res. 28, 437–448.

Zhou, M., Huntley, M.E., 1997. Population dynamics theory of plankton based on biomass spectra. Mar. Ecol. Prog. Ser. 159, 61–73.

Zimmerman, R.A., Biggs, D.C., 1999. Patterns of distribution of sound-scattering zooplankton in warm- and cold-core eddies in the Gulf of Mexico, from a narrowband acoustic Doppler current profiler survey. J. Geophys. Res. 104 (C3), 5251–5262.